Design of Low-Power Wide-Area Networks at Sea

MICHIEL SANDRA
MASTER´S THESIS
DEPARTMENT OF ELECTRICAL AND INFORMATION TECHNOLOGY
FACULTY OF ENGINEERING | LTH | LUND UNIVERSITY

Design of Low-Power Wide-Area Networks at Sea

Michiel Sandra
michiel.sandra@gmail.com

Department of Electrical and Information Technology
Lund University

Supervisor: Anders J Johansson

Assistant Supervisor: Sara Gunnarsson

Examiner: Fredrik Rusek

June 29, 2020

Printed in Sweden
Tryckeriet i E-huset, Lund

Abstract

The development of low-power wide-area (LPWA) technologies has opened up for the deployment of wireless networks for new Internet of Things (IoT) applications. One of these is the monitoring of buoys at sea, which tend to detach due to ice, stormy weather or collision with boats, etc. The main unknown for this application is the behavior of the wireless channel in different sea states and weather conditions, especially at low antenna heights. In this thesis, the impact of various parameters and effects on the wireless channel at sea is studied by means of a literature study, simulations and measurements with a custom-built setup. With this setup, the path loss and fading at sea was measured using point-to-point LoRa links and compared with published models. Additionally, the coverage of the existing networks at sea was tested in the surroundings of Malmö harbor. The results of this thesis showed disagreement with a published model used for ship communication, pointing out the need for further research in this area.

Acknowledgements

First of all, I would like to thank my supervisors, Anders J Johansson and Sara Gunnarsson, for their support and enthusiasm during this project. They were always available and happy to help. In addition, I would like to thank the communications engineering group for including me in the group, which made my stay in Sweden even better. I would also like to thank Harsh Tataria for helping me with some theoretical questions, and Christoffer Cederberg for the support on the hardware side. Furthermore, I would like to thank Sigfox and Telia for sponsoring parts of the hardware. At last, I would like to thank all the organizations and people involved in making my exchange with Lund University possible.

Popular Science Summary

At sea, navigation and hazard marking buoys detach due to ice, stormy weather or collision with boats. An electronic device could be mounted to the buoys to monitor their location and send an alert if the buoy moved out of place. Therefore, a wireless network must be available or could be deployed at sea. There are different types of buoys and for some types of buoys the system should last for ten years because this is the life span of the buoy. A specific type of wireless network, low-power wide-area network (LPWAN), is highly suitable for this application. There are two possibilities for using this kind of network. First, the existing networks could be used, e.g. narrowband Internet of Things (NB-IoT), Sigfox, The Things Networks (TTN). Alternatively, a custom LPWAN can be deployed. An essential part of gaining insight into the design of LPWANs at sea is the model describing the attenuation of a wireless signal as a function of the distance, also known as the path loss model. The signal strength also fluctuates, known as fading, and it is therefore also crucial to know the character of these fluctuations. In these kinds of applications, the antenna height is also very low, making it different from ship communication. Hence, the goal of this thesis is to have a better understanding of the path loss and fading for low antenna height applications at sea. Additionally, the coverage of the existing networks is tested. A literature study, simulations, and measurements were carried out to achieve these goals. For the measurements, a custom setup was built.

The simulations were based on a published model and lead to the following conclusions. First of all, frequency is the most dominant parameter; the higher the frequency, the lower the range. Secondly, there is no influence of the antenna height for larger distances. Thirdly, the effect of the size of the sea waves is limited. At last, the salinity and temperature of the sea surface have little impact. During the measurements, an area of four kilometers was covered in the area of Malmö harbor with a transmitter and receiver height of 2.65 m and 0.35 m, respectively. The measurement results lead to two conclusions. First of all, the results showed disagreement with the published model, pointing out the need for further research in this low antenna height applications. Second, NB-IoT and Sigfox provide coverage in the tested area. Besides that, the measurement setup has also demonstrated the feasibility of deploying an LPWAN at sea and is a promising step forward when digitizing the sea.

Table of Contents

List of Figures

List of Tables

Acronyms

3GPP 3rd Generation Partnership Project.

AWS Amazon Web Services.

BER bit error rate.

BPSK binary phase shift keying.

BW bandwidth.

CDF cumulative distribution function.

CIR channel impulse response.

CR error correction rate.

CRC cyclic redundancy check.

CSS chirp spread spectrum.

ECDF empirical cumulative distribution function.

FEC forward error correction.

IoT Internet of Things.

ISI intersymbol interference.

ISM industrial, scientific and medical.

LNA low noise amplifier.

LOS line of sight.

LPWA low-power wide-area.

LPWAN low-power wide-area network.

LPWANs low-power wide-area networks.

LTE Long Term Evolution.

MAC medium access control.

MAE mean absolute error.

MCL maximum coupling loss.

MPC multipath component.

MPCs multipath components.

OFDM orthogonal frequency division multiplexing.

PA power amplifier.

PDP power delay profile.

PER packet error ratio.

PRR packet reception ratio.

QPSK quadrature phase shift keying.

RMSE root mean square error.

RX receiver.

SC-FDMA single-carrier frequency division multiple access.

SF spreading factor.

SRD short range device.

TOA time on air.

TTN The Things Network.

TX transmitter.

Chapter 1
Introduction

In the past few years, developments in the Internet of Things (IoT) have been increasing exponentially. By 2030, the number of connected IoT devices is expected to be over 50 billion [7]. Embedded devices can be deployed to optimize processes, make our lives easier, safer, etc. Furthermore, they are often energy-restricted and require wireless connectivity. With the development of low-power wide-area (LPWA) technologies like LoRa, Sigfox, and NB-IoT, connecting embedded devices becomes more energy-efficient at long distances, creating opportunities in the deployment of wireless networks in new application areas, like at sea.

1.1 Background and motivation

At sea, navigation and hazard marking buoys tend to detach due to ice, stormy weather or collision with boats, etc. An embedded device could be mounted on the buoys to monitor their location and send an alert if a buoy is out of place. By having the buoys automatically reporting their position and status, safety levels at sea can be increased and money saved by reducing the control intervals. The major requirement for such a system is that the wireless link must stay reliable even in the worst conditions, because then a buoy is more likely to detach. Due to the practical constraints of some types of buoys, the system can be limited to battery power only. Furthermore, the life-span of the system should be around ten years.

To satisfy the above-mentioned requirements, LPWA technologies can be implemented of which there are two possibilities to do so. The first one is to use the existing low-power wide-area networks (LPWANs) such as NB-IoT, SigFox, etc., of which the network infrastructure is already provided. This could be interesting for small-scale deployments. The second one is to deploy a custom network, for which the LoRa technology can be used. The last one could be particularly interesting for the situation where the buoys are out of range of the existing networks. Some possibilities for the implementation of a custom network are that the base stations could be placed close to the coastline with high gain antennas, or the buoys could be interconnected, forming an ad-hoc network.

The main question that arises when designing such a system is what the coverage of the existing networks is, and what coverage can be achieved with a custom network. Note that coverage is defined such that one has coverage if the relia-

bility requirement is fulfilled. Finding an answer to these questions can be quite challenging. Propagation effects at sea like reflection, divergence, scattering, shadowing, and diffraction loss, but also line of sight (LOS) obstruction due to boats, can influence the coverage [6].

1.2 Project aims and methodology

The overall goal of this thesis is to give the stakeholders insights into the deployment of wireless IoT application at sea. Two stakeholders of this project are Sjöräddningssällskapet (SSRS) and Copenhagen Malmö Port (CMP). This thesis will focus on the path loss and fading at sea because these are the still unknown aspects in designing an IoT network at sea, and are different in other environments. Besides that, the coverage of the existing networks will also be tested. This thesis tries to achieve this goal using a five-point plan:

1. An investigation and simulation of published path loss models (Chapter 2)
2. A study of the most popular LPWA technologies (Chapter 3)
3. The development of a measurement setup / prototype (Chapter 4)
4. Measurements of the path loss and coverage test of the existing networks (Chapter 4)
5. Comparison of the path loss measurements with the models from literature (Chapter 5)

1.3 Related work

Researchers in [8][9] already performed coverage tests with LoRaWAN at sea. Their results seem promising but they ignore the long-term behavior and the influence of the sea states, since the measurements were taken during one day. Furthermore, the researchers in [10] already measured a range of approximately 4 km using LoRa point-to-point in a coastal area (not at sea) with a transceiver height of only 1.5 m. Also, the results of the application in [11], using LoRa point-to-point links in an aquatic environment, seem promising.

The idea for this master's degree project is based upon a student project within the course Embedded Systems 2 at KU Leuven (Belgium) in 2019. The assignment was to build a system that could send a message if a buoy was out of place. During the first hours of operation, the students encountered some problems with the connectivity. Besides that, a similar project at the harbor by Malmö was halted because the connectivity seemed unreliable. These two examples show the need for further research into the connectivity of energy-restricted embedded systems in an open-sea environment.

Chapter 2

Channel properties of open-sea radio propagation

2.1 Introduction

A channel in wireless communication can have several different meanings [12]. It is a layer of abstraction in a wireless communication system through which a signal or data can flow. Different properties characterize each type of channel. Next to the propagation channel, other types of channels are the baseband radio channel, digital channel, etc.

This chapter starts with an introduction of a few principles in wireless communications engineering, followed by a literature study and theoretical analysis on the channel properties of open-sea radio propagation and the parameters that affect the channel.

2.1.1 Link budget

To estimate the coverage of an LPWAN, the maximum path loss (MPL) of radio infrastructure can be calculated starting from the link budget equation (2.1) [13], which is applied to simple wireless communication system, like in Figure 2.1. With the value for the MPL, the maximal distance between the receiver and transmitter can be estimated using a path loss model, which will be explained in Section 2.2.

$$P_{RX} = P_{TX} - L_{f,TX} + G_{a,TX} - L_p + G_{a,RX} - L_{f,RX} \tag{2.1}$$

where P_{TX} is the power at the transmitter and P_{RX} the power at the receiver in dBm. $L_{f,TX}$ and $L_{f,RX}$ are the feeder losses at the transmitter and receiver side, respectively, in dB. $G_{a,TX}$ and $G_{a,RX}$ are the antenna gains at the transmitter and

Figure 2.1: A simple wireless communication system

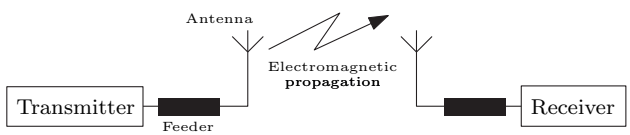

receiver side in dBi, respectively, assuming broadside transmission/reception. L_p is the attenuation in power due to an electromagnetic wave propagating through space. In this thesis, L and G are always positive.

The minimal signal level required to receive a message is the receiver sensitivity S_{RX} in dBm. This is usually a property of the receiver module and is provided by the manufacturer in the data sheet. The S_{RX} is equal to the sum of the input-referred noise level N at the receiver and the minimal signal-to-noise $(S/N)_{min}$ ratio required to demodulate the signal:

$$S_{RX}\,[\text{dBm}] = N\,[\text{dBm}] + (S/N)_{min}\,[\text{dB}] \tag{2.2}$$

Where $(S/N)_{min}$ is determined using a quality measure like bit error rate (BER) or packet error ratio (PER) of, for example, 1%. The $(S/N)_{min}$ will mainly depend on the transceiver's hardware, the modulation technique, and the channel coding or redundancy. For example, the LoRa PHY uses forward error correction (FEC) to improve the quality of the link.

On the other hand, the noise level N is affected by the electromagnetic noise in the surroundings picked up by the antenna, the system bandwidth BW of the transceiver, the temperature, and the hardware of the whole radio system. The latter includes cables, amplifiers, etc. The noise performance of the entire radio system is characterized by the total noise figure NF. Following is an equation that is commonly used for estimating the minimal noise floor:

$$N\,[\text{dBm}] = 10\log_{10}(k \cdot T_0 \cdot 1000) + NF + 10\log_{10}(BW) \tag{2.3}$$

With NF in dB, k the Boltzmann constant, T_0 the reference noise temperature equal to 290 K and BW the system bandwidth in Hz.

Now, the maximum path loss MPL can be calculated as:

$$MPL = P_{TX} - S_{RX} + G_{a,TX} + G_{a,RX} - L_{f,TX} - L_{f,RX} \tag{2.4}$$

The 3rd Generation Partnership Project (3GPP) also uses the term maximum coupling loss (MCL) which does not consider the antenna gains and feeder losses:

$$MCL = P_{TX} - S_{RX} \tag{2.5}$$

2.1.2 Multipath propagation

If both antennas can 'see' each other, there is a line of sight (LOS) connection, which is favorable in most situations. However, the signal can also propagate via many different paths due to reflection, scattering or diffraction. The components of the transmitted signal are called multipath components (MPCs). Each MPC can have a different amplitude, delay (runtime of the signal), phase, and direction of arrival [14].

One drawback of multipath propagation is that two or more rays can interfere at the receiver. For example, if there are two paths and if the difference in length between them is equal to a multiple of $\lambda/2$, and if the electromagnetic waves are equal in amplitude, the two paths will cancel each other out. Thus, no signal will be received.

Multipath propagation can also cause intersymbol interference (ISI). Each of the MPCs arrives at a different time at the RX, which can lead to a dispersion of the signal where successive symbols can interfere and thereby lead to errors [14].

The effects of multipath propagation can be assessed using the channel impulse response (CIR) or power delay profile (PDP). The fading effects can also be included in the path loss model, like in the case of a two-path model. The impact of a reflective surface or obstacle can also be assessed more qualitatively by the concept of Fresnel zones [14].

The open-sea is a multipath environment because the sea is a rough reflective surface. Research has shown that radio wave propagation over the sea is affected by ducts such as surface ducts, elevated ducts, and evaporation ducts [15]. These ducts cause diffraction of electromagnetic waves.

2.1.3 Fading

Changes in the transceiver environment, such as different positions, orientation, weather, obstacles, etc. can cause changes in signal attenuation. The general term used for these fluctuations in the signal attenuation is fading. In literature, fading is usually divided into large-scale and small-scale fading [14], where large and small relates to the wavelength. Small-scale fading can be caused by multipath propagation, and shadow fading is usually a form of large-scale fading, which occurs when a big obstacle obstructs the LOS path. Then, the radio wave propagates around the obstacle due to diffraction at the object's edge, but the signal attenuation will be larger compared to a LOS scenario.

Figure 2.2: Fading margin

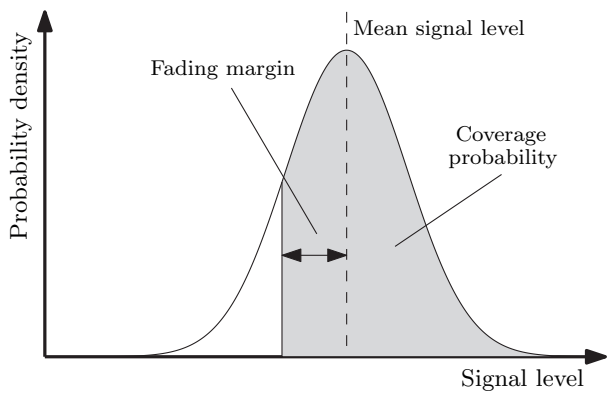

Because these changes in signal strength can be quite random and hard to predict in a deterministic way, fading is usually modeled in a statistical sense. For example, the signal level can be Gaussian distributed, as in Figure 2.2. The fading margin is a margin that is used to calculate the coverage of a mobile communication system, and the higher the required reliability, the larger the fading margin. The mean signal level is determined using a path loss model.

At sea, changes in weather conditions (e.g., change in sea state), height/tilt of the antenna, or boats obstructing the LOS will result in fading.

2.2 Path loss modeling

A path loss model describes the signal attenuation between two wireless devices, e.g., a node and a gateway, and is essential to estimate the coverage of a mobile communication system. The most fundamental path loss model in radio communication is the free space loss factor [14]:

$$L_p = \left(\frac{4\pi d}{\lambda}\right)^2 \tag{2.6}$$

or in dB:

$$L_p[\text{dB}] = 20\log_{10}\left(\frac{4\pi d}{\lambda}\right) \tag{2.7}$$

In Equations (2.6) and (2.7), λ is the wavelength in meter, and d is the distance in meter between TX and RX.

Because the sea is a rough reflective surface, multiple components of the transmitted signal are received at the receiving antenna, also called multipath propagation. Therefore, a two-path path loss model, as in Equation (2.8), is more appropriate as used in [6]. Equation (2.8) slightly differs from the one included in [6], as it is more correct.

$$L_p = \left(\frac{\lambda}{4\pi d_{dir}} + R \cdot \frac{\lambda}{4\pi(d_{dir} + d_{diff})} \exp\left(j\,\frac{2\pi d_{diff}}{\lambda}\right)\right)^{-2} \tag{2.8}$$

where d_{dir} is the distance between TX and RX, d_{diff} is the difference in length of the direct and reflected path, and R is the reflection coefficient. Note that the maximal distance can only be calculated using this model if the antennas are omnidirectional, or if the gain of the antennas is the same for the direct and reflecting wave. This matter is further discussed in Section 2.2.4.

The model proposed in [6] is based on a two-path model but also takes propagation phenomena like rough surface reflection, beam divergence, shadowing, and diffraction loss into account. Because this model shows an agreement with their measurements, it is promising for this project and will be discussed in-depth in this chapter. Another advantage of this model is that it is deterministic. With a deterministic model the effect of the different parameters can be simulated. For example, for finding the most optimal antenna height. For a complete overview of existing literature models for over-the-sea radio communication, the reader is referred to [16].

There are also three-path loss models, taking the effect of evaporation ducts into account, which can enhance the received signal strength. Hence, the phenomenon is very popular in the research community. However, no further attention will be given to this, because these effects are only noticeable for frequencies above 3 GHz [15].

2.2.1 Round earth geometry

The geometry and variables based on [17] used in the following sections are depicted in Figure 2.3. The input variables for the geometry are the antenna heights

h_1, h_2 and the distance d between the antennas projected on the earth's surface, all with the unit m.

Figure 2.3: Round earth geometry

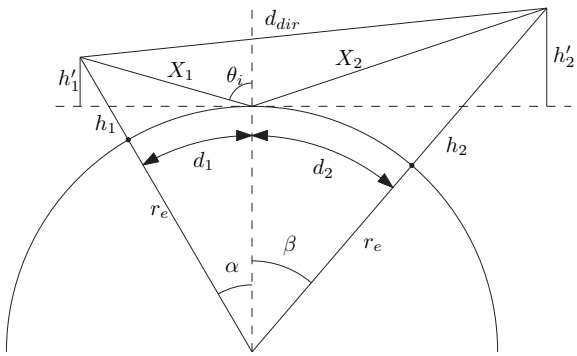

Following relations can be obtained:

$$d_{diff} = X_1 + X_2 - d_{dir} \tag{2.9}$$

$$d = d_1 + d_2 \tag{2.10}$$

$$h'_1 = h_1 - 0.5\, r_e\, \alpha^2 \tag{2.11}$$

$$h'_2 = h_2 - 0.5\, r_e\, \beta^2 \tag{2.12}$$

$$\theta_e = \arcsin\left(\frac{h'_1}{X_1}\right) = \frac{\pi}{2} - \theta_i \tag{2.13}$$

where

$$d_{dir} = \sqrt{(r_e + h_1)^2 + (r_e + h_2)^2 - \xi} \tag{2.14}$$

$$\xi = 2(r_e + h_1)(r_e + h_2)\cos\left(\frac{d}{r_e}\right) \tag{2.15}$$

X_1, X_2, α and β can be obtained from following system of equations:

$$\frac{(r_e + h_2)^2 - r_e^2 - X_2^2}{X_2} = \frac{(r_e + h_1)^2 - r_e^2 - X_1^2}{X_1} \tag{2.16}$$

$$\alpha + \beta = \frac{d}{r_e} \tag{2.17}$$

$$X_1^2 = (h_1 + r_e)^2 + r_e^2 - 2(r_e + h_1) r_e \cos(\alpha) \tag{2.18}$$

$$X_2^2 = (h_2 + r_e)^2 + r_e^2 - 2(r_e + h_2) r_e \cos(\beta) \tag{2.19}$$

This system can be numerically solved using iteration. Above calculations are only valid if there is a LOS connection, or $d < d_{LOS,max}$, where

$$d_{LOS,max} = r_e \cdot \left(\arccos\left(\frac{r_e}{r_e + h_1}\right) + \arccos\left(\frac{r_e}{r_e + h_2}\right)\right) \tag{2.20}$$

If $d > d_{LOS,max}$, then the geometry simplifies as depicted in Figure 2.4. Here, following relations are valid:

$$d_1 = \sqrt{2r_e k_e h_1} \tag{2.21}$$

$$d_2 = \sqrt{2r_e k_e h_2} \tag{2.22}$$

$$d_3 = d - d_1 - d_2 \tag{2.23}$$

$$X_1 = \sqrt{(r_e + h_1)^2 + r_e^2 - 2(r_e + h_1) r_e \cos(d_1/r_e)} \tag{2.24}$$

$$X_2 = \sqrt{(r_e + h_2)^2 + r_e^2 - 2(r_e + h_2) r_e \cos(d_2/r_e)} \tag{2.25}$$

d_{dir} now becomes:

$$d_{dir} = X_1 + X_2 + d_3 \tag{2.26}$$

Figure 2.4: Round earth geometry

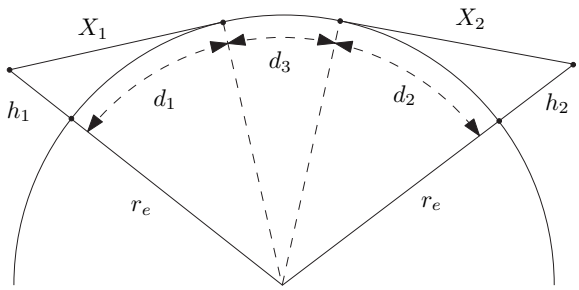

2.2.2 Properties of the sea surface

Electrical properties

The electrical properties of the earth's surface can be characterized by three physical quantities [1]:

- Magnetic permeability μ [N/A^2]
- Electrical permittivity ϵ [F/m]
- Electrical conductivity σ [S/m]

These measures can be used to describe radio wave propagation mechanisms. However, in calculating the Fresnel reflection coefficient, the complex relative permittivity is used, and is defined as,

$$\overline{\epsilon_r} = \epsilon_r' - j\epsilon_r'' = \frac{\epsilon}{\epsilon_0} - j\frac{\sigma}{\omega\epsilon_0}, \tag{2.27}$$

where ϵ_0 is the vacuum permittivity and equal to $8.85 \times 10^{-12}\,\mathrm{F\,m^{-1}}$. For the value of the magnetic permeability, [1] assumes $\mu = \mu_0 = 4\pi \times 10^{-7}\,\mathrm{N/A^2}$.

In [1], methods for the complex relative permittivity of sea (saline) water ϵ_{sw} are provided, which is a function of the frequency f, temperature $T\,[°\mathrm{C}]$ and, salinity $S\,[\mathrm{g/kg}$ or ppt].

The typical salinity values are 35 g/kg for the North Sea and 31 g/kg for the Baltic Sea [18], depicted in Figure 2.5. The effect of a change in temperature is illustrated in Figure 2.6.

Figure 2.5: Complex relative permittivity of sea water as a function of frequency for different salinity values [1] ($T = 5\,°\mathrm{C}$)

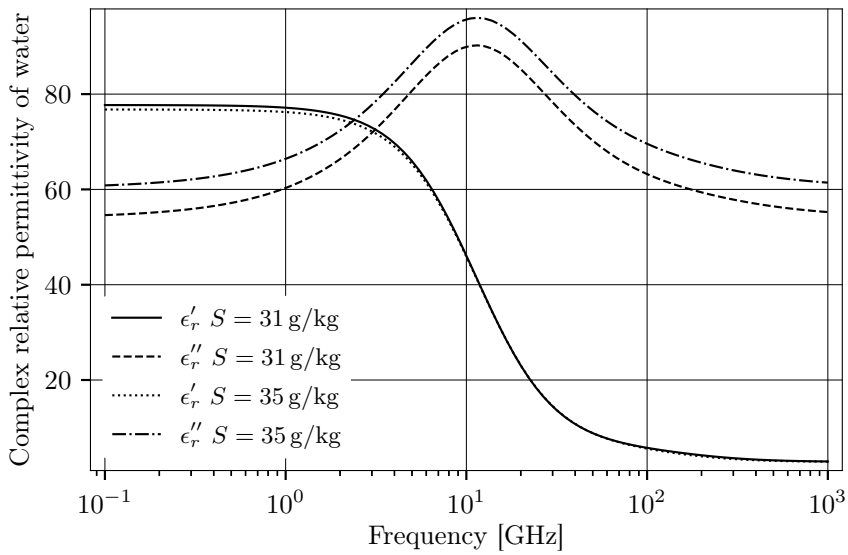

Figure 2.6: Complex relative permittivity of sea water as a function of frequency for different temperature values [1] ($S = 31\,\mathrm{g/kg}$)

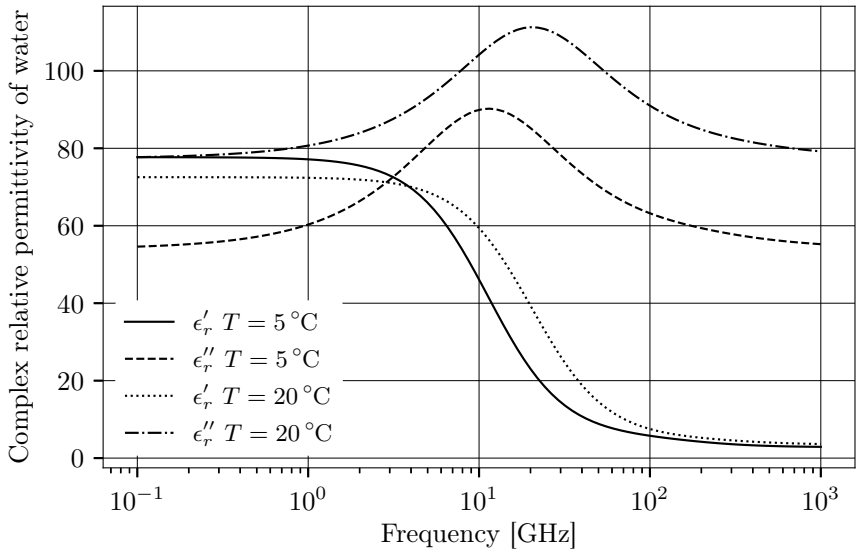

Wave height

Modeling the behavior of sea waves in a deterministic way is a complex task. For channel modeling purposes, the sea surface is assumed to be normal distributed with a mean of zero and characterized by the following parameters [6][19][20]:

- The standard deviation of the surface slope distribution β_0 in rad
- The standard deviation of the wave height distribution σ_h in m

The relation between the two parameters is given by the following equation [20]:

$$\beta_0 = \frac{2\sigma_h}{l} \tag{2.28}$$

Here, l is the correlation length of the sea waves in meters. In [19], the authors provided a method to derive β_0 from an experimental set of sea wave height data that was collected over a long period. Typical values for β_0 are $0.04 - 0.07$ when the waves are $1 - 4\,\mathrm{m}$ high. Another measure is the Douglas sea scale, which categorizes certain values for the sea height in different degrees [4], as presented in Table 2.1. Although there is no direct relation to the REL model, it can be used to categorize experimental data.

Degree	Height(m)	Description
0	no wave	Calm (glasssy)
1	$0 - 0.10$	Calm (rippled)
2	$0.10 - 0.50$	Smooth
3	$0.50 - 1.25$	Slight
4	$1.25 - 2.50$	Moderate
5	$2.50 - 4.00$	Rough
6	$4.00 - 6.00$	Very rough
7	$6.00 - 9.00$	High
8	$9.00 - 14.00$	Phenomenal

Table 2.1: Douglas sea scale [4]

2.2.3 Round earth path loss model

The authors of [6] modified the two path model (2.8) and included other models to take the following effects into account:

- Reflection from a rough sea surface R_{rough}
- Shadowing effect S_{fun}
- Divergence effect Δ
- Diffraction loss L_{diff} in dB

The authors of this model called it the round earth loss (REL) model. For this thesis, the symbols are a modified for consistency. This results in the following equation for the path loss:

$$L_p[\text{dB}] = -20\log_{10}\left(\frac{\lambda}{4\pi d_{dir}} + R_{tot}\cdot\frac{\lambda}{4\pi(d_{dir}+d_{diff})}\exp\left(j\,\frac{2\pi\,d_{diff}}{\lambda}\right)\right) + L_{diff} \tag{2.29}$$

$$R_{tot} = S_{fun}\cdot R_{rough}\cdot\Delta \tag{2.30}$$

It is obvious that beyond the horizon, the second term in (2.29) becomes 0 since there is no reflected ray anymore. The parameters for this model are:

- Carrier frequency f_c in Hz
- The standard deviation of the surface slope distribution β_0 in rad
- The standard deviation of the wave height distribution σ_h in m
- Salinity of the sea surface S in g/kg
- Sea surface temperature T in °C
- Antenna height h_1 and h_2 in m

Reflection from a rough surface

The rough reflective sea surface causes a lot of reflections, which can lead to fading and distortion of the signal, thus decreasing link quality. The Kirchhoff theory [14] provides an equation for the effective refection coefficient for a Gaussian distributed surface. One drawback of this model is that it does not consider shadowing effects, which become significant at low antenna heights. Moreover, the reflected signal from the rough surface can be decomposed in a coherent (specular) and incoherent (diffuse) component due to the scattering of the sea surface. The coherent component has a constant phase difference with the direct component phase, while the phase of the incoherent component is random. The Kirchhoff model considers the reflected wave *on average* [12]. However, the authors of [19] presented a method to calculate the probability density function for the total (coherent and incoherent) signal strength. This means that the fading margin can be calculated but these calculations are quite extensive and time consuming, so they are not included in the thesis. On the other hand, an experimental evaluation of the fading depth could be more useful.

$$R_{rough} = R \cdot \exp\left[-2\left(\frac{2\pi\sigma_h \cos\theta_i}{\lambda}\right)^2\right] \tag{2.31}$$

Here, R is equal to the Fresnel reflection coefficient, which depends on the polarization of the electromagnetic wave. This is also the only factor in this model that depends on the polarization. The Fresnel reflection coefficient can be calculated using the following equations:

$$R_\perp = \frac{\cos\theta_i - \sqrt{\overline{\epsilon_r} - \sin^2\theta_i}}{\cos\theta_i + \sqrt{\overline{\epsilon_r} - \sin^2\theta_i}} \tag{2.32}$$

$$R_\parallel = \frac{\overline{\epsilon_r}\cos\theta_i - \sqrt{\overline{\epsilon_r} - \sin^2\theta_i}}{\overline{\epsilon_r}\cos\theta_i + \sqrt{\overline{\epsilon_r} - \sin^2\theta_i}} \tag{2.33}$$

where subscripts $\perp$ and $\parallel$ indicate the polarization perpendicular and parallel to the incident plane, respectively. In Figure 2.7, the power coefficient $r = |R|^2$ and the change in phase $\phi = \arg(R)$ are plotted. It is interesting to see that at high incident angles (or at low elevation angles, due to low antenna height), the phase of both components is shifted 180 degrees. If only one of the components would shift 180 degrees, circular polarized antennas could be used because this phase shift changes the direction of polarization. So, the reflected wave would not be observed at the receiver, increasing the link's quality. The conclusion is that at high incident angles, no antenna polarization is favorable.

Shadowing effect

Due to the roughness of the sea surface, there is a chance that some points on the sea surface are not visible for both transmitting and receiving antennas because other sea waves shadow the points. This effect is prominent at low elevation angles. Therefore, the shadowing coefficient proposed in [21] was included in

Figure 2.7: Fresnel reflection coefficient ($T = 8\,^{\circ}\mathrm{C}$ en $S = 31\,\mathrm{g/kg}$)

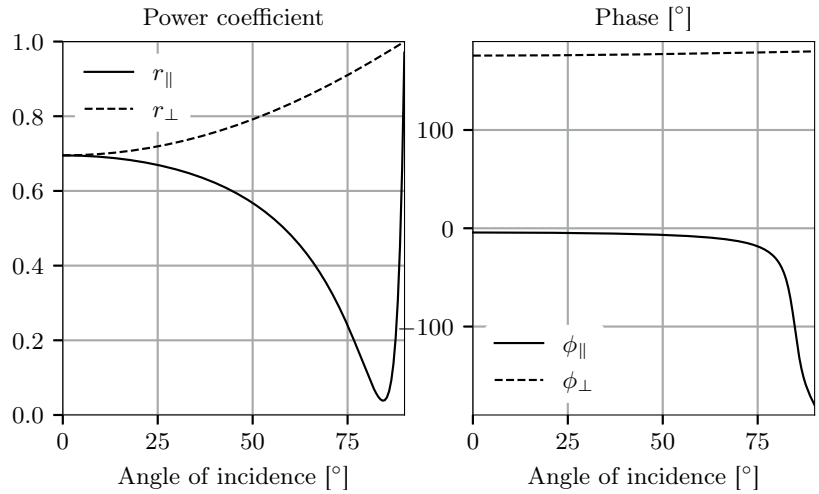

several models [6][19][22].

$$S_{fun} = \frac{1 - 0.5\,\mathrm{erfc}\left(\frac{\cot\theta_i}{\sqrt{2}\beta_0}\right)}{\Lambda(\cot\theta_i) + 1} \tag{2.34}$$

$$\Lambda(\cot\theta_i) = \frac{1}{2}\left(\sqrt{\frac{2}{\pi}}\frac{\beta_0}{\cot\theta_i}\exp\left[-\left(\frac{\cot\theta_i}{\sqrt{2}\beta_0}\right)^2\right] - \mathrm{erfc}\left(\frac{\cot\theta_i}{\sqrt{2}\beta_0}\right)\right) \tag{2.35}$$

Divergence effect

Because of the earth curvature, the power density of the reflected ray will decrease more than if the earth be flat. Therefore, the divergence effect was included in the REL model [6]:

$$\Delta = \frac{1}{\sqrt{1 + \frac{2d_1 d_2}{r_e(h_1' + h_2')}}} \tag{2.36}$$

This equation is only applicable if $h_1' > 0$ and $h_2' > 0$, otherwise Δ is equal to 0.

Diffraction loss

At the open sea, wireless communication is still possible beyond the horizon because of diffraction. However, the diffraction loss needs to be taken into account. In this thesis this is done based on the calculations in [23], which are different from the REL model in [6]. Now, Figure 5 from [23] is used. The condition for using this nomogram was that the antenna height has to be lower than approximately

12 m for frequencies around 900 MHz. Hence, the diffraction loss is not affected by the antenna height.

The value for L_{diff} was calculated using Equation (2.37) and (2.38). Equation (2.38) is an approximation from the graph in Figure 13 in [23].

$$\zeta_a = \frac{\frac{2\pi d}{\lambda}}{\left(\frac{2\pi k r_e}{\lambda}\right)^{2/3}} \tag{2.37}$$

$$L_{diff} = 10^{1.429 \cdot \log_{10}(\zeta_a) - 0.5804} \tag{2.38}$$

where k is the ratio of the effective earth's radius and the true earth's radius. In this thesis, we assume $k = 1$. The rest of the variables are already introduced in the preceding sections.

Simulations

In Figures 2.9 to 2.15 the influence of the different parameters are illustrated. In each figure, there is only one parameter that changes. All the other parameters are according to Table 2.2.

From Figure 2.9, it can be concluded that the frequency plays the most important role in the path loss. So, a lower frequency would be more preferable. However in practice, the size of the antenna is limited, so it could be challenging to design a good antenna for this frequency. Generally, if two antennas made for different frequencies would have the same size, than the one for the higher frequency would have a higher gain. Figures 2.10 and 2.11 lead to the conclusion that the the antenna heights don't influence the path loss on longer distances, if both antenna height are below a certain value [23]. In addition, the effect of the sea state is limited, as demonstrated in Figure 2.14 to 2.16. On longer distances, there is no influence at all. Furthermore, a variation of the sea surface temperature or the salinity does not affect the path loss, as shown in Figure 2.12 and 2.13.

2.2.4 Round earth path loss model considering the radiation pattern of the antennas

The calculated and plotted values for the path loss in Section 2.2.3 consider the radiation pattern of both receiving and transmitting antenna to be isotropic. If not, the attenuation of the direct and reflected signal will differ. Consequentially, the link budget in Equation (2.1) cannot be used. However, the antenna gain contribution can be included in the round earth loss model (Equation (2.29) and (2.30)) as follows:

$$P_{RX} = P_{TX} - L_f - L_p \tag{2.39}$$

With P_{TX} the power at the transmitter and P_{RX} the power at the receiver in dBm. L_f is equal to the total feeder losses of the system in dB. L_p is now equal

to:

$$L_p = -20\log_{10}\left(\frac{\lambda \cdot G_{a,dir}}{4\pi d_{dir}} + R_{tot} \cdot \frac{\lambda \cdot G_{a,refl}}{4\pi(d_{dir}+d_{diff})}\exp\left(j\,\frac{2\pi\, d_{diff}}{\lambda}\right)\right) \tag{2.40}$$

$$R_{tot} = S_{fun} \cdot R_{rough} \cdot \Delta \tag{2.41}$$

$$G_{a,dir} = \sqrt{G_{a,1}(\theta_{dir,1},\phi_{dir,1})} \cdot \sqrt{G_{a,2}(\theta_{dir,2},\phi_{dir,2})} \tag{2.42}$$

$$G_{a,refl} = \cdot\sqrt{G_{a,1}(\theta_{refl,1},\phi_{refl,1})} \cdot \sqrt{G_{a,2}(\theta_{refl,2},\phi_{refl,2})} \tag{2.43}$$

where the antenna gain G_a is on a linear scale and the indices TX and RX from Equation (2.1) are replaced by 1 and 2, respectively.

For an ideal dipole antenna, the radiation pattern is equal to:

$$G_a(\theta,\phi) = G_{a,max}\sin^2(\theta) \tag{2.44}$$

using a spherical coordinate system with the antenna along the z-axis, as depicted in Figure 2.8. The antenna gain G_a is on a linear scale. Based on the calculations in Section 2.2.1, values for θ_{dir} and θ_{refl} can be calculated using the following equations:

$$\theta_{dir,1} = \arccos\left(\frac{(r_e+h_2)^2 - d_{dir}^2 - (r_e+h_1)^2}{-2\,d_{dir}(r_e+h_1)}\right) \tag{2.45}$$

$$\theta_{dir,2} = \arccos\left(\frac{(r_e+h_1)^2 - d_{dir}^2 - (r_e+h_2)^2}{-2\,d_{dir}(r_e+h_2)}\right) \tag{2.46}$$

$$\theta_{refl,1} = \arccos\left(\frac{r_e^2 - (h_1+r_e)^2 - X_1^2}{-2\,(r_e+h_1)X_1}\right) \tag{2.47}$$

$$\theta_{refl,2} = \arccos\left(\frac{r_e^2 - (h_2+r_e)^2 - X_2^2}{-2\,(r_e+h_2)X_2}\right) \tag{2.48}$$

For an ideal dipole antenna that is mounted perpendicular to the earth's surface, $G_a(\theta,\phi) \approx G_{a,max}$ for $d > 100\,\text{m}$ in the scenario of the parameters as in Table 2.2. This is demonstrated by calculating the above values for $d = 100\,\text{m}$:

$$\begin{aligned}\theta_{dir,1} &= 88.6\\ \theta_{dir,2} &= 91.32\\ \theta_{refl,1} &= 88.28\\ \theta_{refl,2} &= 88.28\end{aligned}$$

Taking the smallest value for $\sin(\theta)$: $\sin^2(\theta_{refl,1} = 88.28°) = 0.999$.

If the antenna would be mounted on a buoy at sea, then the movement of the buoy needs to be included as well. Next to the radiation pattern, loss due to polarization mismatch should also be considered.

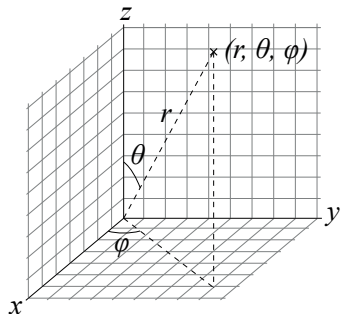

Figure 2.8: Spherical coordinate system [2]

2.2.5 Log-distance path loss model

The log-distance path loss model [14] is another useful model to fit experimental data to:

$$L_p(d) = L_{p,0} + 10\,n\,\log_{10}(d/d_0) + \chi_\sigma \tag{2.49}$$

$$\overline{L_p}(d) = L_{p,0} + 10\,n\,\log_{10}(d/d_0) \tag{2.50}$$

where $L_{p,0}$ is the path loss at d_0, and n is called the path loss exponent. χ_σ describes the fading around the mean path loss and is model as $\mathcal{N}(0, \sigma^2)$. At sea, fading of the signal could be caused by diffuse reflection on the rough sea surface, where the phase and magnitude of these diffuse reflections are random and time-variant. Boats can also obstruct the LOS connection between RX and TX, which can also result in a decrease in signal strength.

2.3 Conclusion

Using the REL path loss model from [6], the influence of various parameters can be put into perspective. From Figures 2.9 to 2.15, it can be concluded that the carrier frequency is the most dominant. The parameters β_0 and σ_h representing the sea state, have little effect on the path loss or are even improving the path loss. However, it must be highlighted that the REL model gives the path loss *on average*, and that other parameters like the sea state could have more influence in terms of fading. On longer distances, diffraction becomes the most important effect and only depends on the frequency if both antennas are below a certain value [23].

Parameter	Value
f_c	868 MHz
β_0	0.008 rad
σ_h	0.25 m
S	31 g/kg
T	15 °C
h_1	2.65 m
h_2	0.35 m

Table 2.2: Default values for the plots of the REL-model

Figure 2.9: Path loss as a function of distance and frequency

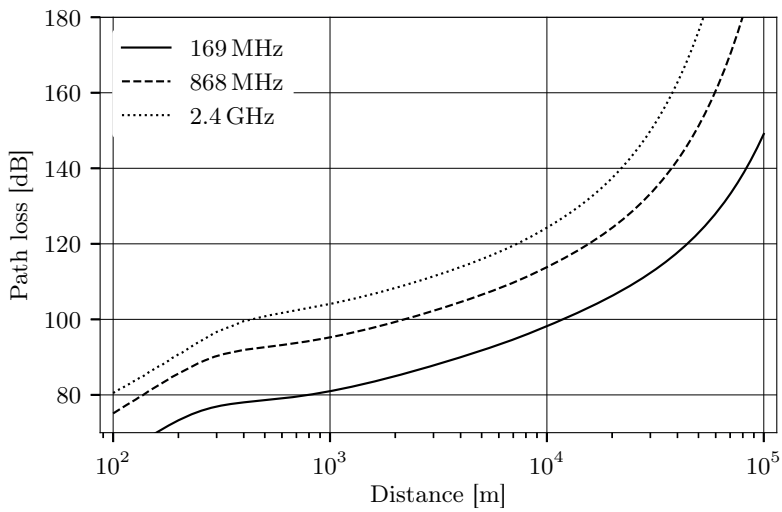

Figure 2.10: Path loss as a function of distance and antenna height (h_1)

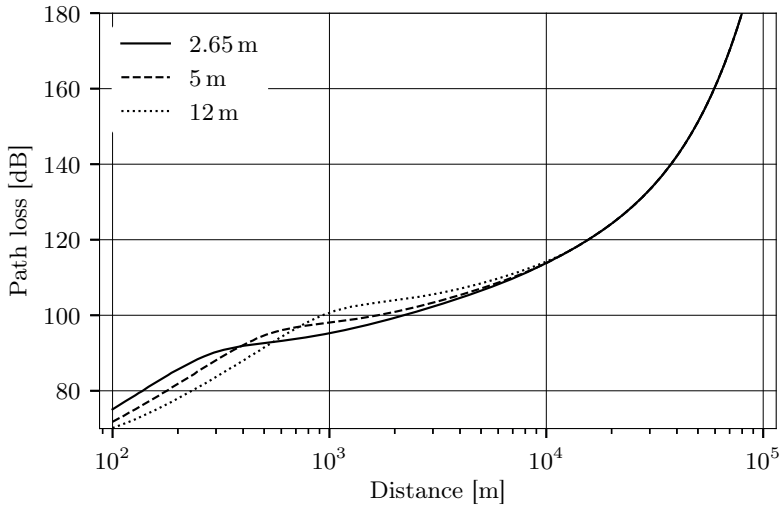

Figure 2.11: Path loss as a function of distance and antenna height (h_2)

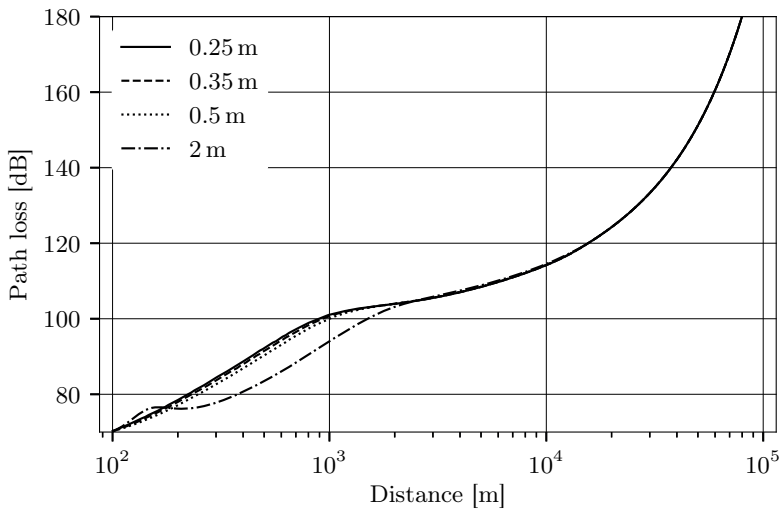

Figure 2.12: Path loss as a function of distance and salinity

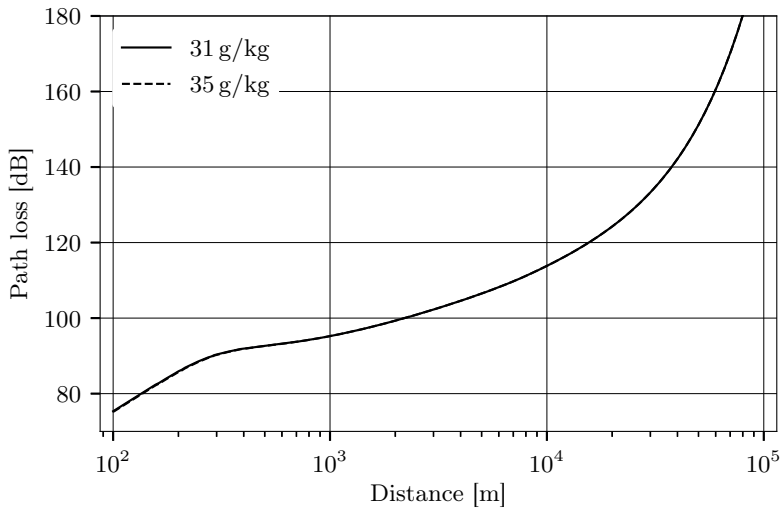

Figure 2.13: Path loss as a function of distance and sea surface temperature

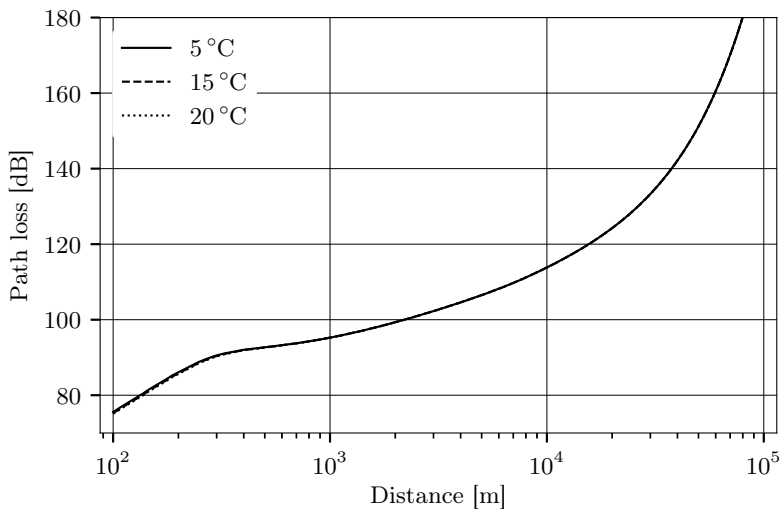

Figure 2.14: Path loss as a function of distance and β_0

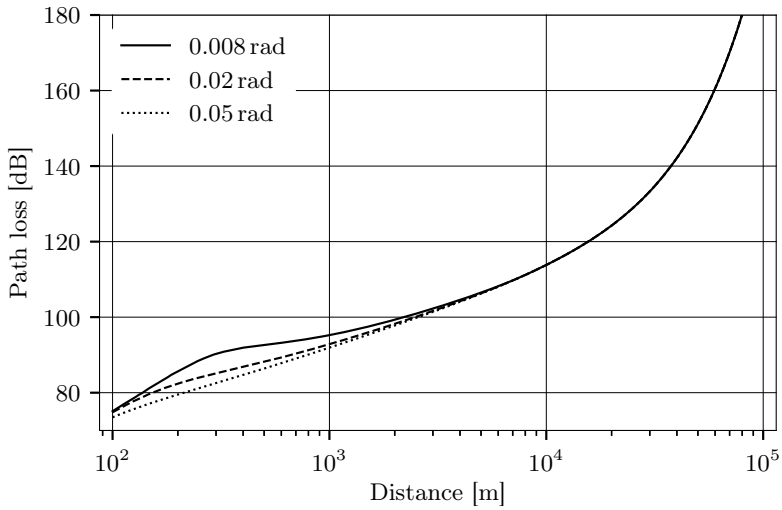

Figure 2.15: Path loss as a function of distance and σ_h

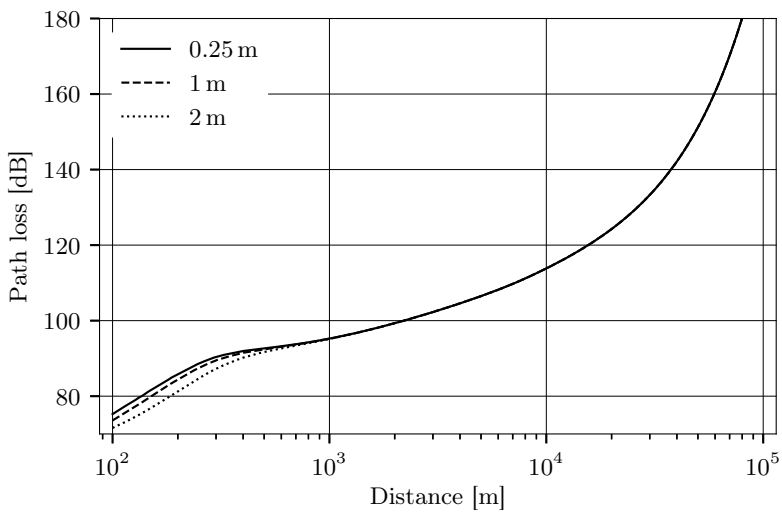

Figure 2.16: Path loss as a function of distance and sea state (σ_h and β_0)

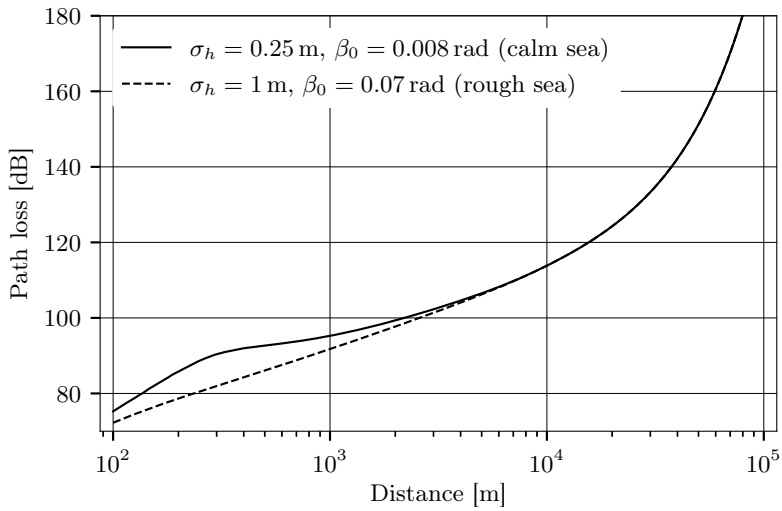

Figure 2.17: Contribution of the different effects to R_{tot} according to the REL model

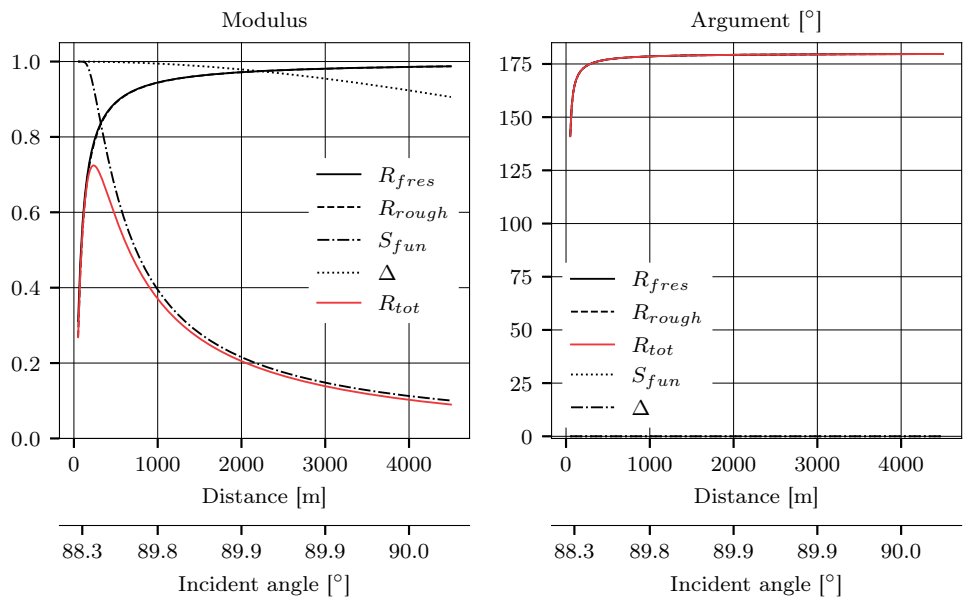

Chapter 3

Low-Power Wide-Area Network technologies

Low-power wide-area networks are a recent innovation in wireless communication that provides wireless connectivity for electronic devices within larger areas, for a low energy cost. Many IoT applications that do not require a high data rate can benefit from this kind of technology. Besides the coverage and energy consumption, features like security, scalability, latency, etc. are also important but are out of scope of this thesis. This chapter gives a brief overview of the most popular low-power wide-area network (LPWAN) technologies (LoRa, Sigfox, and NB-IoT), with a focus on what is relevant for this thesis. There are, of course, other technologies that might be worth looking into.

3.1 LoRa

LoRa (short for long range) is a proprietary modulation scheme that derived of chirp spread spectrum (CSS) modulation [24], developed by Cycleo in 2009, and then sold to Semtech in 2012 [25]. LoRa is also the basis of the crowd-sourced network named The Things Network (TTN), which uses the LoRaWAN medium access control (MAC) protocol, standardized by the LoRa Alliance. Furthermore, everyone can use TTN for free. However, coverage is not guaranteed since most gateways are voluntarily placed by individuals or organizations at sometimes non-preferable locations, like indoors. The advantage of LoRa is that it provides a lot of flexibility in two perspectives. One is that there is a trade-off possible between the link budget and the energy consumption using different configurations, which will be explained later. The second is that LoRa can be deployed for a private network where different types of network topologies like a star or mesh network are possible. The only thing required for using this technology is a LoRa transceiver from Semtech (e.g., the SX1276), which costs, at the moment of writing, around 4 EUR for large volumes.

The three main parameters for making the right trade-off between link budget and energy consumption are the bandwidth (BW), error correction rate (CR), and spreading factor (SF). For example the BW can be configured from 7.8 to 500 kHz, the SF from 6 to 12, and the CR from 1 to 4. Both the BW and SF affect on the link budget, because the $(S/N)_{min}$ depends on the SF, as presented

SF	$(S/N)_{min}$ [dB]
6	-5
7	-7.5
8	-10
9	-12.5
10	-15
11	-17.5
12	-20

Table 3.1: LoRa $(S/N)_{min}$ as a function of the spreading factor [3]

SF \ BW	10.4 kHz	125 kHz	500 kHz
6	-131	-118	-111
7	-134	-123	-116
8	-138	-126	-119
9		-129	-122
10		-132	-125
11	-146	-133	-128
12		-136	-130

Table 3.2: LoRa sensitivity in dBm for different spreading factor SF and RF bandwidth BW, with a correction rate CR of 2, at a packet error rate PER of 1 %

in Table 3.1. These values for the $(S/N)_{min}$ were determined for a packet error ratio (PER) of 1%, under specific circumstances mentioned in the datasheet [3]. Besides that, the noise level N will vary according to the temperature, the system bandwidth and the noise figure of the receiver, and the noise level in the receiver's surroundings. Together with the $(S/N)_{min}$, the sensitivity and link budget can be calculated. Typical values for the sensitivity are also provided in the data sheet. A few configurations are summarized in Table 3.2. However, these numbers are recorded or calculated under specific circumstances or settings and can vary from the actual values. For this reason, practical measurements are more useful.

The LoRa transceivers use forward error correction (FEC) to enhance the reliability of the channel, and so decreasing the packet error ratio (PER). The channel coding can be configured using the CR. Besides that, a 16-bit cyclic redundancy check (CRC) for the payload is also optional. While a higher SF and CR will increase the link budget and the reliability, the data signal's nominal bit rate will decrease. As a result, the energy consumption will be higher for the same payload size.

In Figure 3.1 the LoRa packet structure is presented. For estimating the energy

SF \ BW	10.4 kHz	125 kHz	500 kHz
6	0.420	0.035	0.009
7	0.766	0.064	0.016
8	1.680	0.1152	0.029
9	2.769	0.206	0.051
10	5.538	0.412	0.103
11	9.895	0.823	0.181
12	17.42	1.450	0.362

Table 3.3: TOA in seconds for a LoRa packet of 20 bytes for different SF and BW, in explicit header mode, CRC enabled, 8 programmed preamble symbols and a CR of 2 [3]

consumption, the time on air (TOA) can be used, using following equations [24][3]:

$$T_S = \frac{2^{SF}}{BW} \tag{3.1}$$

$$T_{preamble} = (n_{preamble} + 4.25) \cdot T_S \tag{3.2}$$

$$n_{payload} = 8 + \max\left(\text{ceil}\left[\frac{8PL - 4SF + 28 + 16CRC - 20IH}{4(SF - 2DE)}\right](CR + 4), 0\right) \tag{3.3}$$

$$T_{TOA} = T_{preamble} + n_{payload} \cdot T_S \tag{3.4}$$

where:

- T_S is the symbol rate; the time it takes to send a symbol
- $n_{preamble}$ represents the number of programmed preamble symbols
- PL is the size of the payload in bytes
- SF is the spreading factor
- $IH = 0$ when the header is in explicit header mode, $IH = 1$ is in implicit mode
- $DE = 1$ when $T_S > 16\,\text{ms}$, $DE = 0$ otherwise
- CR is the coding rate
- $CRC = 1$ when CRC is enables, $CRC = 0$ otherwise

In Table 3.3, some values for the TOA are calculated, which can be used to calculated the energy consumption, which will be described later on. Now, the packet's energy consumption can be added to the energy consumption of the other components of the device to estimate the life span. It must also be highlighted that if LoRaWAN is used, the TOA will be more significant for the same amount of data sent, due to the protocol's overhead.

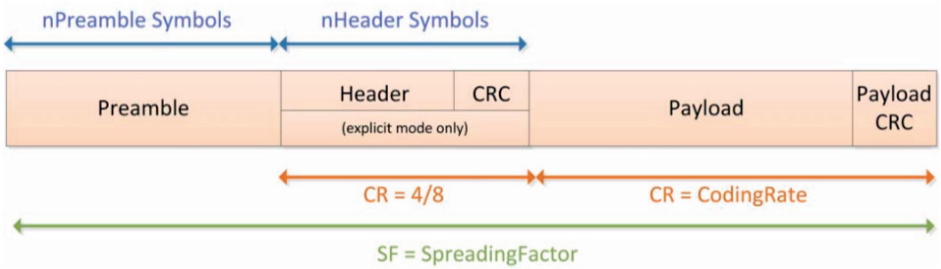

Figure 3.1: LoRa packet structure [3]

3.2 NB-IoT

NB-IoT (short for narrowband Internet of Things) is an extension of the current cellular technology to provide connectivity for low-power devices. It was first introduced in the 3rd Generation Partnership Project (3GPP) Release 13, the organization responsible for the standardization of telecommunication systems. At the time of writing, there is coverage for NB-IoT across most of Europe [26], due to its compatibility with the existing Long Term Evolution (LTE) infrastructure. As it is a cellular technology, a SIM card and subscription are required to join the network, besides a transceiver module. A transceiver module, like the U-Blox SARA-N211, costs around 14 EUR for large volumes. The price is higher than those for LoRa and Sigfox, due to the higher complexity of the technology.

The physical layer of NB-IoT is based on the one for LTE since they can coexist. NB-IoT uses orthogonal frequency division multiplexing (OFDM) and single-carrier frequency division multiple access (SC-FDMA) as downlink and uplink transmission schemes, respectively, with binary phase shift keying (BPSK) or quadrature phase shift keying (QPSK) modulation schemes. There are three coverage classes, which result in an MCL of 144 dB, 158 dB and 164 dB with a maximum transmit power of 23 dBm, so the maximal sensitivity is equal to −141 dBm. NB-IoT also has a maximum bit rate of 26 kbps and 66 kbps, for downlink and uplink, respectively.

In terms of the energy consumption, 3GPP published some simulations in technical report TR45.820. For a coupling loss of 164 dB the estimated service life of a device with a battery capacity of 18 kJ is equal to 2.5 years, if the device sends a message of 50 bytes every 2 hours.

3.3 Sigfox

Sigfox is a low-power IoT service provider and was founded in 2010. The strength of Sigfox is that it provides a complete service and that the radio modules are cheap because of the low complexity of the technology. For example, the WSSFM10R1 Sigfox module costs around 3 EUR. Sigfox also owns its base stations and is thereby independent of cellular technology. However, coverage is still limited to central Europe and the bigger cities all around the world. One of the drawbacks of Sigfox

is that the data rate is low; 100 bps and 600 bps for uplink and downlink, respectively, using a binary phase shift keying (BPSK) modulation scheme. Due to the regulations on radio equipment in Europe (see later), the maximum length of a message (payload length) is restricted to 12 bytes, and the total amount messages per day to 140. The TOA of a Sigfox message of 12 bytes is 6.24 s, because Sigfox uses time and frequency diversity to optimize the reliability. The same uplink message is sent three times after each other at three different frequencies.

3.4 Frequency bands and regulations

When looking at the spectrum the LPWANs operate in; they can be divided into unlicensed and licensed. NB-IoT operates in the licensed bands, while LoRa and Sigfox can operate in the unlicensed short range device (SRD) and industrial, scientific and medical (ISM) bands. In this section, only the regulations for Europe are considered. In Table 3.4, the E-UTRA bands are summarized where NB-IoT operates in.

E-UTRA Band	Uplink	Downlink
3	1710 - 1785 MHz	1805 - 1880 MHz
8	880 - 915 MHz	925 - 960 MHz
20	832 - 862 MHz	791 - 821 MHz

Table 3.4: NB-IoT bands in Europe [5]

On the other hand, for the Sigfox and LoRaWAN networks the ERC Recommendation 70-3 [27] applies, see Table 3.5 and 3.6. This includes that SRDs are limited in terms of radio effective radiated power (e.r.p.) and spectrum access (duty cycle). The e.r.p. in dBm is equal to $P_{TX}[\text{dBm}] + G_{TX}[\text{dBi}] - 2.15$. The SRDs can be further categorized, depending on the application. The two relevant categories for this project are:

- Non-specific short range devices (annex 1)
- Tracking, tracing and data aquisition (annex 2)

In the case of the buoys, annex 2 would apply. Although, TTN and Sigfox are applying annex 1. Sigfox uses band h1.5, and TTN uses bands h1.4, h1.6, and h1.9. In this project, we focus on the bands near 868 MHz, so the same antenna could be used for comparing the technologies.

3.5 Energy consumption

In Table 3.8, the energy consumption for sending a message, with a payload size of 20 and 50 bytes, for different configurations and technologies is presented. There is aimed for the larger values of the MCL. Hereafter, it is explained how the values for Table 3.8 are calculated.

For NB-IoT, the results of the technical report (TR45.820) from 3GPP are used. A device with a battery of 18 kJ lasts for 2.5 years when sending a message

Frequency Band		Maximum e.r.p.	Spectrum access
h0	862-863 MHz	14 dBm	duty cycle $\leq 1\,\%$
h1.0	863-870 MHz	14 dBm	duty cycle $\leq 0.1\,\%$
h1.1	865-868 MHz	14 dBm	duty cycle $\leq 1\,\%$
h1.2	863-870 MHz	14 dBm	duty cycle $\leq 0.1\,\%$
h1.3	863-865 MHz	14 dBm	duty cycle $\leq 0.1\,\%$
h1.4	865-868 MHz	14 dBm	duty cycle $\leq 1\,\%$
h1.5	868-868.6 MHz	14 dBm	duty cycle $\leq 1\,\%$
h1.6	868.7-869.2 MHz	14 dBm	duty cycle $\leq 0.1\,\%$
h1.7	869.4-869.65 MHz	27 dBm	duty cycle $\leq 10\,\%$
h1.8	869.7-870 MHz	7 dBm	No requirement
h1.9	869.7-870 MHz	14 dBm	duty cycle $\leq 10\,\%$

Table 3.5: ERC Recommendation 70-3 (annex 1) for bands near 868 MHz

Frequency Band		Maximum e.r.p.	Spectrum access
c1	865-868 MHz	500 mW	duty cycle $\leq 2.5\,\%$
c2	870-874.4 MHz	500 mW	duty cycle $\leq 2.5\,\%$

Table 3.6: ERC Recommendation 70-3 (annex 2) for bands near 868 MHz

of 50 bytes every. In the report, the authors also mentioned that the power in sleep mode is equal to 0.015 mW. So, the energy per message can be approximated as:

$$E_m = \frac{E_{\text{battery}} - E_{\text{sleep}}}{\text{number of messages}} = \frac{18\,\text{kJ} - 2.5 \cdot 365 \cdot 24 \cdot 3600 \cdot 0.015\,\text{mW}}{2.5 \cdot 365 \cdot 12} = 1.54\,\text{J} \tag{3.5}$$

Here, it is assumed that the time in sleep mode is much longer than the time in active or transmitting mode, and that the energy consumed by the microcontroller is negligible in comparison to the energy consumed by the transceiver. For calculating the energy consumption of a LoRa message, Equation (3.4) and the values from Table 3.2 are used. Hence, the energy can be calculated as the multiplication of the TOA and the power consumption in transmit mode:

$$E_m = P_{TX} \cdot T_{TOA} \tag{3.6}$$

The same equation is used for Sigfox but with a different transmit power consumption. The values for the transmit power consumption are summarized in Table 3.7. NB-IoT is not included in the list since the estimation is not so simple as in (3.6).

Note that these calculations are an approximation; the energy for the MCU and sensors is not included. For a more accurate comparison, the energy consumption has to be measured.

3.6 Conclusion

In terms of coverage and reliability, the MCL can be used for comparison. Here, all technologies, except when using TTN, show a similar value for the MCL. However,

Device	Transmit power	Power consumption in transmit mode	Power consumption in sleep mode
LoRa (SX1276)	13 dBm	95.7 mW	0.66 µW
	20 dBm	396 mW	
Sigfox (Wisol)	14 dBm	178.2 mW	6.6 µW
PA (NXP BGS8L2)	n/a	16.8 mW	3.3 µA

Table 3.7: Power consumption per device (IC)

one should consider that the values for the MCL are not precisely comparable. These values are obtained for a specific quality (reliability) measure, e.g., the BER or PER. The MCL values are adopted from [28], but they did not mention how these values were calculated or measured, and for what quality measure.

When determining the technology with the best coverage at sea, one should also consider that the base stations of NB-IoT, Sigfox, and TTN could be located in different and unfavorable environments (and height), resulting in an extra loss. Therefore, it is better to test the coverage in a practical situation.

In terms of energy consumption, it is clear that LoRa offers the most flexibility. The general trend is that the higher the sensitivity, the higher the energy consumption.

Another conclusion out of this chapter is that it is useful to look at the power restrictions in the ERC recommendation. For example, a power amplifier (PA) could be used at the transmitter side to boost the MCL. Furthermore it has been shown that the internal power amplifier (PA) of the SX1276 LoRa transceiver is less efficient than the external PA.

	NB-IoT	**LoRa P2P (w/o PA)**	**LoRa P2P (w/ PA)**	**LoRa (TTN)**	**Sigfox**
Spectrum	880-915 MHz 832-862 MHz	869.4-869.65 MHz	869.4-869.65 MHz	865-868 MHz 868.7-869.2 MHz 869.7-870 MHz	868-868.6 MHz
Type of band	licensed, LTE	unlicensed, SRD	unlicensed, SRD	unlicensed, SRD	unlicensed, SRD
Transmit power	23 dBm	20 dBm	26 dBm	13 dBm	14 dBm
System bandwidth	180 kHz	10.4 kHz	10.4 kHz	125 kHz	192 kHz
SF	n/a	11	8	12	n/a
MCL	164 dB	168 dB	164 dB	149 dB	160 dB
Energy per message (50 bytes)	1.5 J	9.0 J	0.46 J	0.26 J	n/a
Energy per message (12 bytes)	n/a	3.5 J	0.17 J	0.14 J	1.1 J

Table 3.8: Energy consumption comparison of the different LPWA technologies.

Chapter 4
Measurements

To assess the coverage of LPWANs at sea, measurements are a must. In contrast to a theoretical investigation or a simulation, measurements provide real-world, practically useful results in a limited amount of time.

The aims of the measurements are:

1. To potentially validate the REL path loss model described in Chapter 2.
2. To characterize the fading at sea and determine the fading margin.
3. To test the coverage at sea of the existing networks (NB-IoT, SigFox, and TTN)

The purpose of the first two aims is to estimate the coverage when deploying a custom low-power network at sea. The third aim is to evaluate to what extent the existing networks can be used, thus avoiding the additional network infrastructure.

The first two aims can be achieved by using a LoRa P2P connection and capturing the Received Signal Strength Indicator (RSSI) values at multiple TX-RX distances. The test for the coverage can be based on the packet reception ratio (PRR).

The reason to use the off-the-shelf radio modules instead of using channel sounder for the channel measurement is twofold. First of all, using low-power radio technology allows for measuring for several weeks. This is particularly interesting because a wireless channel can be time-variant. Especially at sea, where the weather conditions could have a big impact on the channel. Secondly, mounting radio equipment on a buoy is practically constrained, it has to be compact and waterproof. The disadvantage of not using a channel sounder is that the measurements are less accurate, and no phase information is provided.

4.1 Measurement setup

To realize the above mentioned measurements, two waterproof boxes had to be built: one master box and one slave box. The master box contains all the technologies described in Chapter 3. The slave box is made to provide the LoRa P2P connection and will always be listening for messages. If the master box sends a LoRa message and if the slave box can receive it, then the slave box will send a message back to the master box.

Figure 4.1: The architecture of the master box

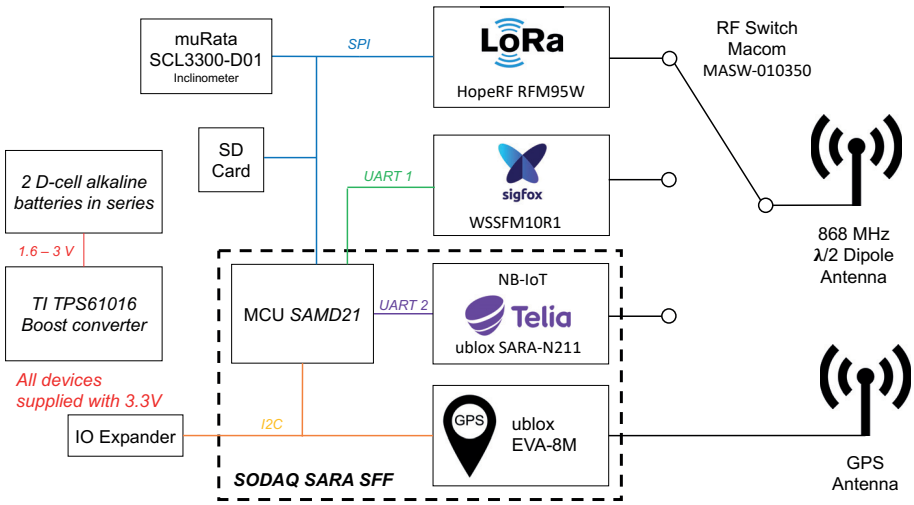

4.1.1 The master box

The master box is realized using a combination of existing modules and PCBs, and self-built boards attached to an interconnection board, except for the RF switch. This kind of design allows for rapid development and is suitable for a test system. The architecture of the master box is depicted in Figure 4.1. All devices are powered with a supply voltage of 3.3 V. The practical realization of the interconnection board and the connected boards is shown in Figures 4.2 and 4.3. This piece is then mounted on a 3D-printed frame that also holds the batteries, as shown in Figure 4.4. Next, the mounting part is enclosed in a 110 mm PVC pipe interconnection piece with two closing pieces at each end. The 3D-printed mounting frame is attached using 2 M4 screws to one of the bottom closing pieces with a rubber ring in between. The final physical appearance is shown in Figure 4.5. The 868 MHz antenna is placed on top in the center of the box. Next to the antenna, a waterproof button is provided. The function of the button can be programmed in the software.

Some initial tests with this kind of housing showed that this housing is really waterproof. Besides that, PVC is a chemically inert material which is also preferable in a harsh environment as the open sea. In the following sections the separate parts of the master box are discussed more in-depth.

Batteries

For this test system, alkaline D-cel batteries are used (VARTA Industrial Pro 4020). These provide an energy capacity of approximately 70 kJ in a compact package and cost no more than 1.6 EUR. The nominal voltage of these batteries is 1.5 V. When in use, the voltage drops linearly with the remaining energy capacity to around 0.8 V. The reported capacity rating in the datasheet is equal to

Figure 4.2: Practical realization of the interconnection board for the master box (front)

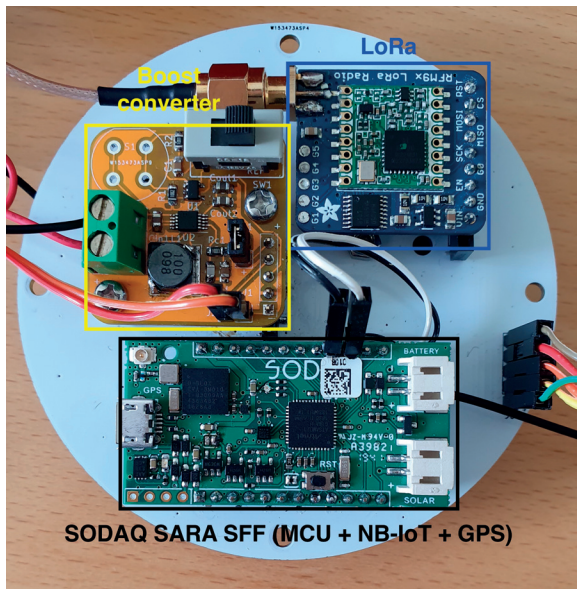

Figure 4.3: Practical realization of the interconnection board for the master box (back)

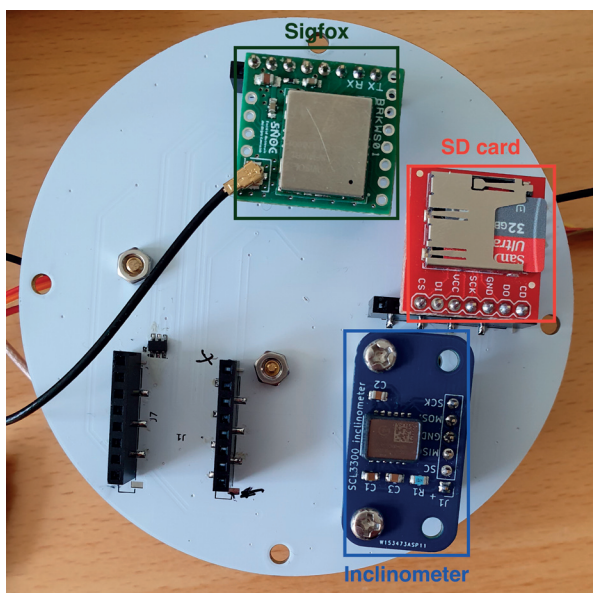

Figure 4.4: Practical realization of the master box without the waterproof housing

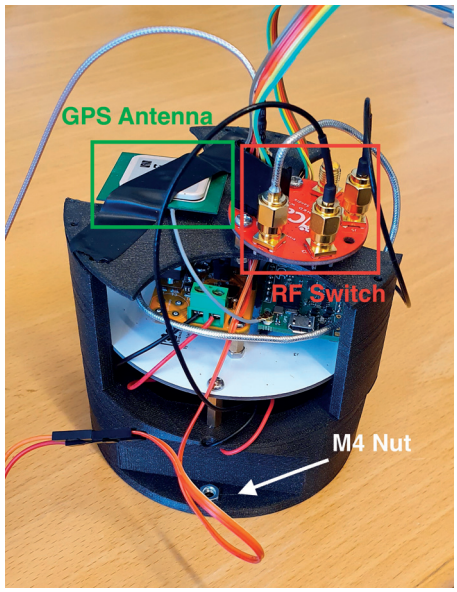

Figure 4.5: The physical appearance of the master box

Figure 4.6: Schematic of the power supply unit

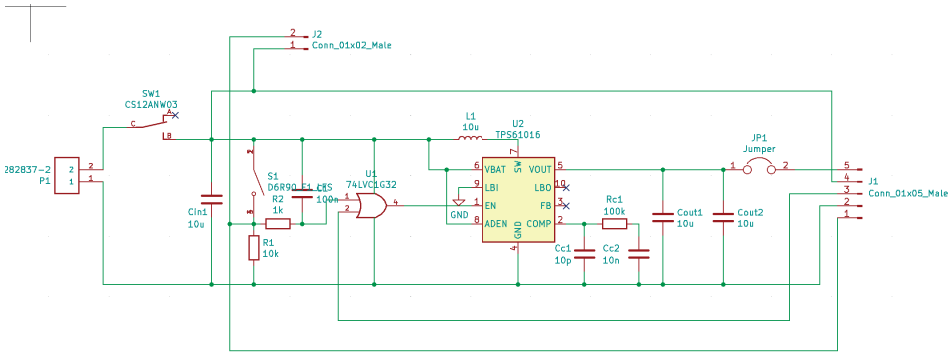

17 Ah when discharged with a high impedance. Hence, the energy capacity can be calculated as

$$E = \frac{1.5\,\mathrm{V} + 0.8\,\mathrm{V}}{2} \cdot 17\,\mathrm{Ah} \cdot 3600\,\mathrm{s} \approx 70\,\mathrm{kJ}$$

The disadvantage of alkaline batteries is that the capacity is temperature-sensitive. The capacity will decrease with temperature. Lithium batteries are less temperature-sensitive but are much more expensive. For example, a similar lithium battery, the Saft LS33600, has an energy capacity of 220 kJ and comes for 35 EUR, making it seven times more expensive for the same energy capacity. The number of batteries was limited by the dimensions of the box. Two batteries could fit in.

Power supply unit

To anticipate to the decrease in battery voltage over time, a power supply unit with a boost converter had to be built. The TPS61016 from Texas Instruments was chosen because it is intended for these battery systems and has high efficiency. The schematic of the power supply unit is shown in Figure 4.6. The components' values were calculated using the equations and recommendations in the datasheet for an output current of 200 mA. Furthermore, there are also connections for measuring the battery voltage, measuring the whole box's energy consumption, and turning off the PSU when the battery voltage drops below 0.8 V. The latter was implemented using an OR-gate. The box is turned on using a single throw switch. The button must be held until the MCU has started up and set the signal to the OR-port high.

Micro controller

The microcontroller used for this project was integrated on the NB-IoT development board, the SODAQ SARA SFF, that was sponsored by Telia. The board features the Atmel SAMD21G18 microprocessor, which uses a 32-bit ARM Cortex M0+ core and has some low-power features. For programming the microcontroller, the Arduino framework is used for rapid and convenient development.

Radio modules

Sigfox and Telia respectively sponsored the radio modules for Sigfox and NB-IoT. For LoRa, a breakout board from Adafruit featuring a HopeRF RFM96W radio is used. The code for programming was inspired or adapted from libraries on GitHub. For the RSSI measurement of the LoRa P2P link, the built-in feature of the radio is used.

In the development of the box, there was an attempt to calibrate this RSSI measurement by connecting the master and slave box with a step attenuator. Unfortunately, the low signal levels were hard to measure. It seems that, due to leakage at the connectors or transceiver board, a weak signal bypassed the attenuator. Therefore, signals with a power below the power of this bypassing signal could not be captured. To anticipate this problem, the slave box was put in an shielded mobile antenna coupling device from Rode&Schwarz. Hence, the leakage in the area of the transceiver of the slave box was excluded. However, even if the attenuator was not connected, a signal could still be received. Here, a $50\,\Omega$ terminator was connected to both the master and slave box. By moving the slave and master box apart, the sensitivity could be determined. In the experiment, the lowest signal that could be received was equal to $-114\,\mathrm{dBm}$. However, the reported sensitivity of the device is $-138\,\mathrm{dBm}$.

For the coverage test of the existing LPWANs, values for the base station's signal strength can also be obtained for TTN and NB-IoT. However, it does not provide us with a lot of information about the wireless channel at sea. This is because the base stations are placed at locations where the surroundings could affect the channel. For TTN, the RSSI value can be found in the online dashboard and is, in this case, forwarded to the ThingSpeak server, as later described. In the case of NB-IoT, the `AT+CSQ` command is used to obtain the value for the signal strength.

Inclinometer

To monitor the movement of the box, an inclinometer was installed. If the box were placed to be on a buoy, it would be interesting to measure how a buoy moves. This can provide information about the correlation between the sea state and signal strength. The muRata SCL3300-D01 was chosen because of its excellent noise performance, high stability, and low power consumption. Besides that, the inclinometer also features a temperature sensor.

RF switch

To be able to implement all three technologies in a compact package, an RF switch has to be used. This is also beneficial for the comparison between the technologies, since the same antenna is used. Because the off-the-shelf RF switches are quite big, a custom RF switch board was built. This board features a Macom MASW-010350 SP4T RF switch and can be seen in Figure 4.4. The criteria for the choice was an operating voltage of $3.3\,\mathrm{V}$ and a low current consumption ($< 100\,\mu\mathrm{A}$). This switch operates with a voltage from $-0.5\,\mathrm{V}$ to $7\,\mathrm{V}$, draws about $1\,\mu\mathrm{A}$ of current, and thereby meets the criteria.

Figure 4.7: Coplanar wave guide with ground plane

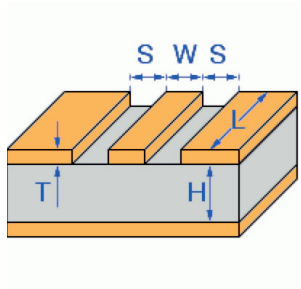

In the design of the PCB for the RF switch, a coplanar wave guide with ground plane is used as transmission line, depicted in Figure 4.7. To realize an impedance of 50 Ω, following values were determined using the KiCAD PCB calculator tool: $W = 1.08\,\text{mm}$, $S = 0.2\,\text{mm}$, $T = 35\,\mu\text{m}$, $H = 1.6\,\text{mm}$.

Antennas

All radio modules are connected to the same 868 MHz $\lambda/2$ dipole antenna, the ANT-868-CW-HW from Linx technologies. The reason to use this kind of antenna is the omnidirectional radiation pattern in the horizontal plane. The GPS antenna Taoglas AP.25E.07.0054A was used because of the combination of the high gain (15 dB) and the limited power consumption (13 mW) of the low noise amplifier (LNA).

Other

In the design, an SD card slot is also provided that can be used for data logging. There is also a connection provided for future testing of the LoRa modules that work on 2.4 GHz, but it is out of scope of the thesis.

4.1.2 The slave box

The design of the slave box is very similar to the design of the master box. It consists of three parts: the power supply unit, the Adafruit LoRa board, and the Sparkfun 9DoF Razor IMU M0 board. The latter is merely used for the microcontroller, which is the same as the one on the SODAQ board. The Arduino framework is also used to program this board.

4.1.3 Cloud interface

For the measurement system, all the data that the radios send must be saved in some way, to process it later on. Besides storage on an SD card, cloud services are used. All the data ends up in the ThingSpeak platform, where the data can be exported to a CSV file. Connecting all the LPWANs to the ThingSpeak servers was

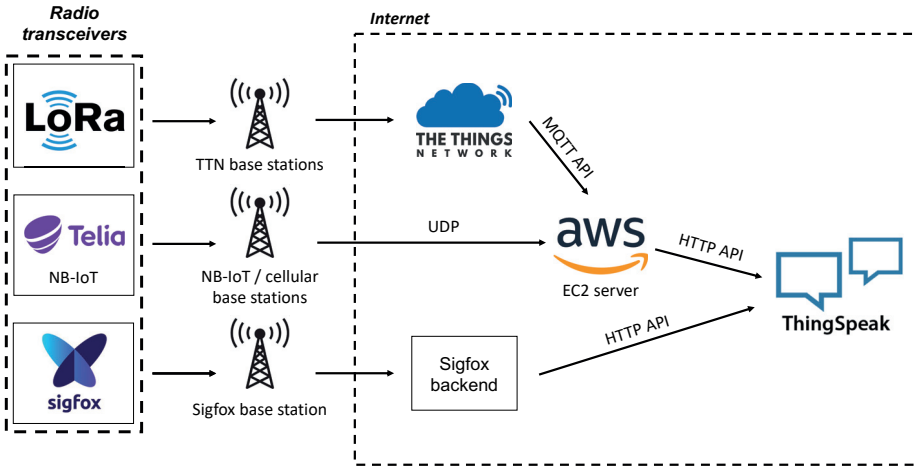

Figure 4.8: Could interface and data collection for the LPWANs

not straightforward. The overall structure of how the systems are linked together is depicted in Figure 4.8.

The server of TTN could not directly be connected to the ThingSpeak server without losing the RSSI information of the messages. Besides that, the ThingSpeak server cannot handle UDP messages. To solve these problem, a little Linux server was developed in Python to correctly interface the all systems. For deploying this server, Amazon Web Services (AWS) was used.

4.2 Measurement campaign

4.2.1 The initial plan

The initial plan for the measurement campaign was first to take the master box out on a boat for path loss measurement and coverage test. The slave box would be placed in the harbor or attached to a buoy. Secondly, the master box would be attached to a buoy for a couple of weeks. Hence, these measurement results would give insights to the character of the fading and the correlation with the weather and sea state. Due to the situation with COVID-19, things did not go as planned, and the plan had to be adjusted.

4.2.2 The adjusted plan

The plan was modified as follows. Instead of a motorized boat, a kayak was used. The disadvantage of using a kayak over a motorized boat is that the testing area is smaller. Another disadvantage is that the lower antenna height on the kayak may not be representable like for the application with the buoys.

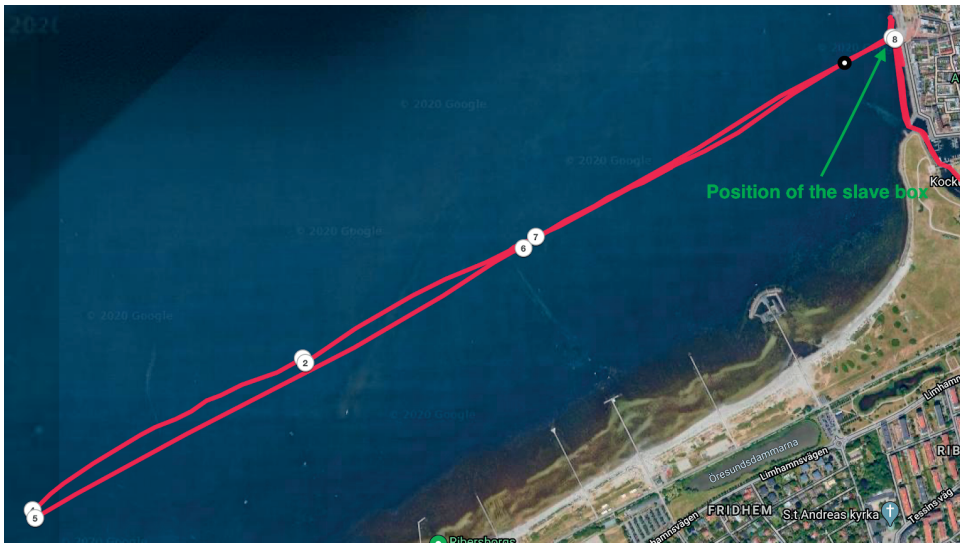

Figure 4.9: Trajectory of the measurement using a kayak

With the kayak, a distance of approximately 4 km has been covered back and forth. The trajectory can be seen in Figure 4.9. The numbers are where the kayak has started or stopped. The trajectory started at the position of the slave box (point 8 on the Figure). The measurements were taken on the 21st of 2020. It was a sunny day, and the sea state was degree 2 on the Douglas scale (Table 2.1). During the kayak trip, a measurement cycle was executed every 20 s. There was also a break approximately every 20 minutes. In the next subsection, the measurement cycle is discussed. The measurement parameters are presented in Table 4.1. The output power of the Sigfox and NB-IoT module was set to 14 dBm, which is the limit according the the ERC recommendations.

Parameter	Value
Number of measurements	178
Master box antenna height	0.3 m
Slave box antenna height	2.65 m
Antenna gain	0 dBi
Antenna radiation pattern	omnidirectional
Transceiver sensitivity	−138 dBm
Output power	17 dBm
Carrier frequency	689.41 MHz
Maximal distance	4234 m
Average temperature	19.5 °C
Maximal tilt of the kayak	22°

Table 4.1: General measurement parameters combined with the parameters of the LoRA P2P connection

4.2.3 The measurement cycle

Approximately every 15 to 25 seconds seconds, the RTC alarm of the SAMD21G18 microcontroller generates an interrupt that starts the measurement cycle:

1. Get the GPS location
2. Set the next alarm
3. Measure the battery voltage
4. Do a LoRa P2P link measurement
5. Measure the tilt of the box using the inclinometer
6. Measure the tilt (inclinometer)
7. Measure the temperature (inclinometer)
8. Send NB-IoT message
9. Send Sigfox message
10. Send LoRa message (TTN)
11. Save all data to SD-card.
12. Go to sleep

Note that the alarm is set after the GPS positioning because calculating the position can vary a few seconds. At any time, an interrupt can be generated by pushing on the button on top which has leads to the same procedure as the alarm interrupt.

To meet the regulations regarding spectrum access step 9 and 10 are only executed every 32 and 64 messages, respectively.

LoRa P2P message

The message that has been used for the LoRa is 18 bytes long. The first byte is an address that is checked if a message is received at both slave and master, to eliminate a message being received that was not coming from the boxes. For power saving, there were also bytes provided in the master-to-slave message for the number of seconds that the slave may sleep before a new message is a sent by the master. Besides that, in the slave-to-master message, the RSSI and SNR values of the preceding slave-to-master message were also sent to the master. The rest of the messages are filled with random values until the length of the message is equal to 18 bytes because experience has shown that a longer packet length results in a more stable RSSI measurement.

Byte	Content
1 - 4	Latitude
5 - 8	Longitude
9	Location ID
10 - 11	Message ID
12	Battery voltage
13 - 14	X-axis tilt
15 - 16	Y-axis tilt
17 - 18	Z-axis tilt
19	Temperature
20 - 21	LoRa P2P RSSI
22	LoRa P2P SNR
23 - 24	NB-IoT signal strength

Table 4.2: Contents of the base message

LPWAN message

For each LPWAN, variants of the base message are used. The structure of the base message is presented in Table 4.2. For Sigfox and TTN, the first 12 and 22 bytes are sent. For NB-IoT, the full base message is sent. The reason behind these choices is that Sigfox is limited to 12 bytes by the network itself. The last 2 bytes are not included in the LoRa message because it makes no sense to send the signal strength of NB-IoT, if no NB-IoT message can be received. With an encoding of the latitude and longitude into 4 bytes, an accuracy of approximately 1 m is achieved.

Furthermore, the *Message ID* and *Location ID* might look over-dimensioned but it can be useful for future measurements.

Energy consumption

For one measurement cycle, the estimated current consumption was about 50 mA for 15 seconds. When the system is not active, the current consumption is equal to 11 mA. Since this design was only for measurement purposes, the energy consumption was not further optimized. The required energy for one cycle every 20 seconds is equal to:

$$E_{cycle} = 3.3\,\mathrm{V}(\cdot 50\,\mathrm{mA} \cdot 15\,\mathrm{s} + 11\,\mathrm{mA} \cdot 5\,\mathrm{s}) = 2.65\,\mathrm{J}$$

Hence, with the two alkaline D-cell batteries, 25.000 measurements are feasible.

If the master box would be mounted on a buoy and a measurement cycle would be performed every 15 minutes, then the box would last for approximately 1900 measurements, or 20 days.

The energy consumption for the slave box was not measured since the master box will always consume more.

4.2.4 Path loss calculation

The path loss L_p in dB is calculated out of the RSSI values of the LoRa P2P connection using the following equation:

$$L_p = -RSSI + P_{TX} - L_f \tag{4.1}$$

where the $RSSI$ and P_{TX} is in dBm, L_f is equal to the total feeder loss of the measurement system in dB. For the LoRa P2P measurement, an L_f of 2 dB was measured using a spectrum analyzer. P_{TX} is equal to 17 dBm.

Chapter 5
Results and discussion

In this chapter, the results of the measurements are presented and compared with the models from literature. The path loss measurements are compared with three models: the REL model, a two-path model with the reflection coefficient as a variable, and the log-distance path loss model. After that, the fading of the channel is discussed.

5.1 Path loss

In Figure 5.1, the measurement data and the REL model from Chapter 2 are plotted. It is clear that the REL model does not agree with the measurements, at least not in the situation where the antenna height is low. For illustration, the path loss is plotted for different values of β_0. Plotting different values for σ_h makes no sense here because the only factor in the REL path loss model that is affected by σ_h is the roughness factor R_{rough}, which can be calculated using Equation (2.31). However, for higher values of θ_i, the exponent in Equation (2.31) goes to zero. Consequentially, the R_{rough} becomes equal to R_{fres}, which is also confirmed in Figure 2.17.

In Figure 5.2 a two-path model is used, with R as a variable. Here, R is considered to be real and negative. This is justified by looking at Figure 2.17: for a distance greater than approximately 500 m, the argument of R_{tot} becomes 180°. One thing to notice is that R tends to increase over distance, which is in contrast to the REL model where the shadowing factor S_{fun} will heavily affect the total reflection coefficient for longer distances, as shown in Figure 2.17. So, S_{fun} is not correct in this type of environment with low antenna height. For comparison, the log-distance model (Equation (2.49)) was also fitted to the measurement data and plotted in Figure 5.3. For the reference distance, $d_0 = 100\,\text{m}$ is chosen, where $L_{p,0} = 75\,\text{dB}$. This is justified because we are only interested in the path loss at hundreds of meters to tens of kilometers. Moreover, d_0 is bigger than the breakpoint distance, which can be approximated by [14],

$$d_{break} \approx \frac{4h_1h_2}{\lambda} = 11\,\text{m} \tag{5.1}$$

Based on the RMSE and MAE values, the log-distance model fits best to the data. This result is particularly interesting because it is the least complex model.

Figure 5.1: Plot of the path loss measurement data of the LoRa P2P links, and the REL model with different values for β_0. The rest of the parameters are according to Table 4.1.

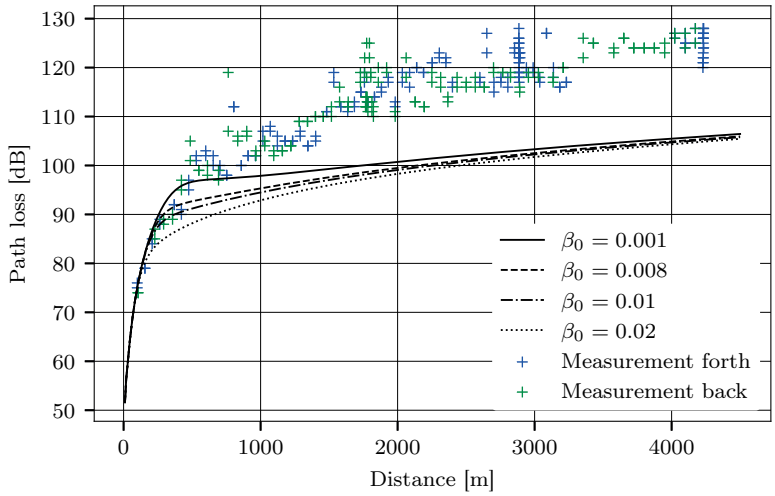

Figure 5.2: Plot of the path loss measurement data of the LoRa P2P links, and the two-path model (Equation (2.8)) with R as a variable

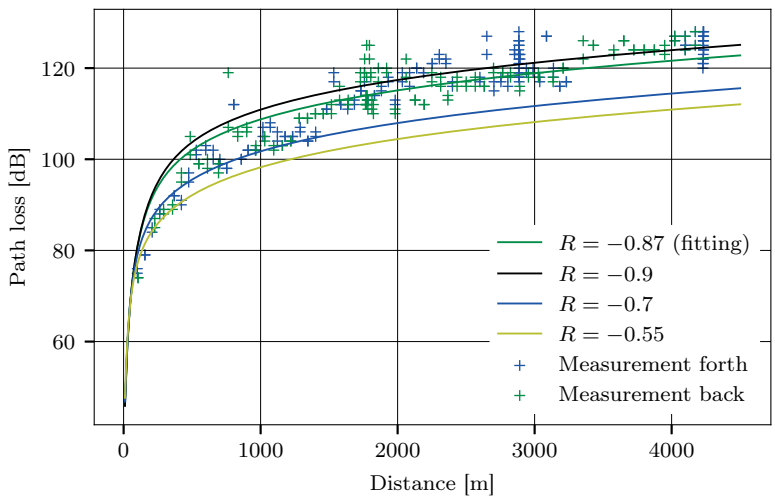

Figure 5.3: Plot of the path loss measurement data of the LoRa P2P links, and the log-distance model (Equation (2.49))

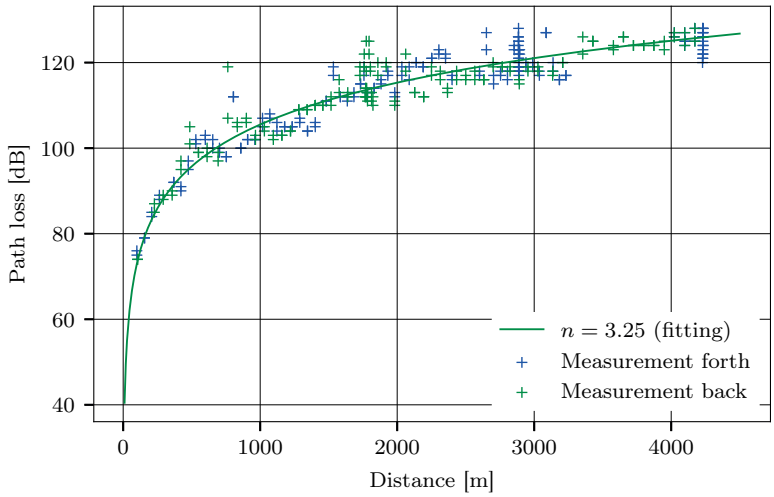

Model	RMSE (dB)	MAE (dB)
REL model	16	15
Two-path model	4.5	3.7
Log-distance model	3.5	2.6

Table 5.1: root mean square error (RMSE) and mean absolute error (MAE) of the fitted model in Figure 5.3, 5.2, and Figure 5.1 with parameters $\beta_0 = 0.008$ and $\sigma_h = 0.25$ because the same weather conditions are considered as in [6]

The models were fitted to the data using the Python `curve_fit` function from the `scipy.optimize` library. The fitting uses the non-linear least squares method. Besides that, no weighting was used for the fitting because the measurement points are quite equally distributed over the distance.

5.2 Packet loss

Table 5.2 summarizes the packet reception ratio (PRR) of the measurements. Unfortunately, all LoRa packages sent to TTN were lost. Although, before the measurements in the kayak club, packages from the TTN network were received. Sigfox has the best PRR but the amount of packages that were sent is much lower compared to the other technologies, which makes the comparison not entirely fair.

In Figure 5.4, the cumulative absolute packet loss is only shown for the LoRa P2P and NB-IoT. Interesting to notice is the loss of packages when the master box was moving away from the slave box, between approximately 3200 m and 4200 m.

Figure 5.4: Cumulative absolute packet loss as a function of distance

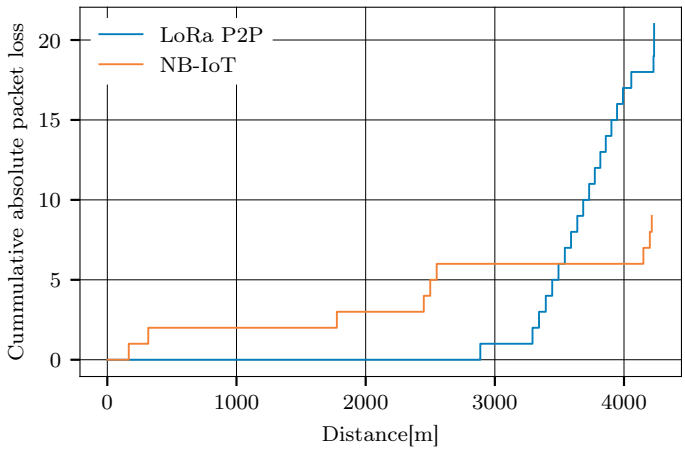

Technology	Packages sent	Packages received	PRR
LoRa P2P	178	157	88 %
LoRa (TTN)	18	0	0 %
Sigfox	9	9	100 %
NB-IoT	178	169	95 %

Table 5.2: Observed packet reception ratio (PRR) during the measurement campaign

This loss is most likely due to a big ship blocking the LOS connection. If we would ignore this loss, only four LoRa packages were lost during the whole measurement. This loss of packages also shows that this star network topology with one base station is not ideal in a realistic scenario. NB-IoT on the other hand, lost nine packages in total. Although, the RSSI of the NB-IoT connection (Figure 5.5) shows that the coverage in the area is good. When testing the device, it became clear that the connection was not so reliable when combining the use of the RF switch and the short message time intervals.

5.3 Fading

The fading of the channel is assumed to be normally distributed around the mean path loss for which the log-distance path loss model is used because it fits the measurements well in comparison to the other models. χ_σ is estimated as follows:

$$\chi_\sigma = \frac{1}{N}\sum_{i=1}^{N}(L_{p,i}(d_i) - \overline{L_p}(d_i))^2 \tag{5.2}$$

Figure 5.5: RSSI measurement of the NB-IoT connection

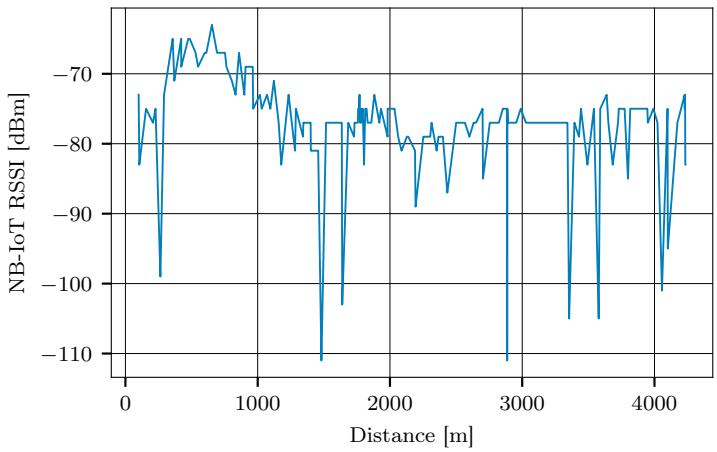

with N the number of path loss measurements, $L_{p,i}$ a path loss measurement sample, and d_i the TX-RX distance of that sample. $\overline{L_p}(d_i)$ is the mean path loss at distance d_i.

The empirical cumulative distribution function (ECDF) of the measurement data and the cumulative distribution function (CDF) are plotted in Figure 5.6from which it can be concluded that the fading can be assumed to be normally distributed. Now the link margin can be determined, which can be calculated using Equation (5.3) for an outage probability p. In this case, the outage probability is the probability that the received signal strength drops below the receiver's sensitivity. Furthermore, the `ppf` (percent point function) for the normal distribution can be used, which is included in the Python `scipy.stats` library.

$$FM = \text{ppf}\,(1-p) \cdot \chi_\sigma \tag{5.3}$$

For example, if there is aimed for an outage probability of 0.1% the link margin becomes 11 dB.

One of the causes of the fading could be due to the up and down movement of the antenna on the waves. Another cause could be the fading due to tilting of the antenna (radiation pattern and polarization mismatch) which is equal to: $10\log(\cos^4(22°)) = -1.31\,\text{dB}$. Hence, the plots in 2.10 and the calculation above show that it is not the complete explanation of measured fading.

5.4 Coverage estimation

In this section, it is shown how the coverage of a custom private network using LoRa technology can be estimated based on the measurement results. Let's assume an application where the location of kayaks is tracked and sent to the mainland. The same setup and configuration is assumed as in the measurement campaign.

Figure 5.6: Cumulative distribution function of the large-scale fading considering the log-distance model as average power

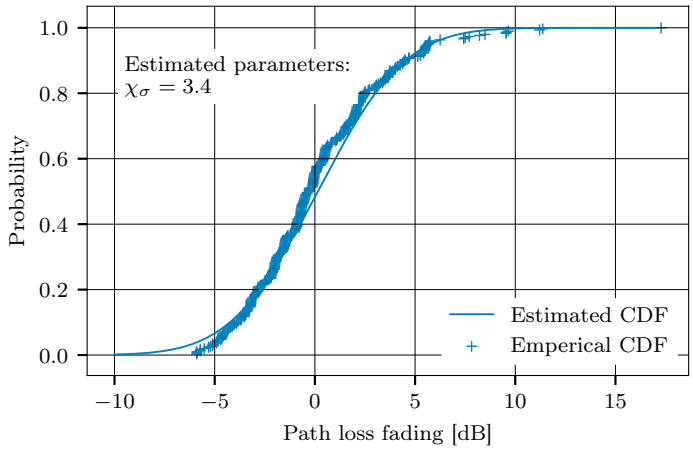

Now, the maximal coverage could be estimated as follows. First, the MPL is calculated with $P_{TX} = 13\,\text{dBm}$, $S_{RX} = -138\,\text{dBm}$, $G_{a,TX} = G_{a,RX} = 0\,\text{dBi}$, $L_{f,TX} = L_{f,RX} = 0\,\text{dB}$

$$MPL = 13 + 138 = 151\,\text{dB} \tag{5.4}$$

Now for the coverage, the distance is calculated for what distance d the $L_p = MPL - FM$, where FM is used from the previous section.

$$d_{max} = 10^{\frac{MCL+FM-L_{p,0}}{10\,n}} \cdot d_0 = 10^{\frac{151+13-75}{10\cdot 3.25}} \cdot 100\,\text{m} = 55\,\text{km} \tag{5.5}$$

However, this result is not realistic, at these distances the diffraction loss has to be taken into account. Furthermore, if the required coverage would be lower, then the required sensitivity would also be lower. As discussed in Chapter 3, the LoRa radios can then be configured to lower the energy consumption.

Chapter 6
Conclusion

In this thesis, the impact of various parameters and effects on the wireless channel at sea is studied by means of a literature study, simulations and measurements with a custom-built setup. With this setup, the path loss at sea was measured using point-to-point LoRa links and compared to the models from literature. In addition, the coverage of the existing networks at sea was also tested in the surroundings of Malmö harbor.

The comparison of measurements and theory lead to the conclusion that the REL model is not applicable to these low antenna height applications. In particular, the shadowing factor in this model seems to be the main cause of the disagreement with the measurements. However, the theoretical investigation of this model gave insight into the effect of different propagation phenomena on the path loss and fading of the channel. Of these phenomena, the diffraction loss affects the path loss on longer distances the most. Furthermore, the frequency is the most dominant parameter, since the diffraction loss only depends on the frequency at low antenna heights.

In the measurements, a distance of 4 km was covered, which was not enough to validate the model for the diffraction loss, but it is something to investigate in future work. Besides the REL model, the path loss data was compared to a log-distance and two-path model. Out of the three models, the log-distance path loss model fits the best to the data according to the RMSE and MAE. However, a good fit with the the two-path model was expected because of the typical two-path environment.

Furthermore, the coverage test showed that the infrastructure of NB-IoT and Sigfox can also provide wireless connectivity at sea although the measurements were conducted close to the shore. Measurements further way from the shore could reveal the practical limit of the coverage of their network infrastructures. No coverage was detected for TTN, most likely due to the limited amount, or unfavorably placed gateways in the area.

The results of this thesis contribute to the future development and deployment of reliable networks at sea, focusing on a custom network using LoRa technology. Therefore, good channel models are essential in order to estimate coverage. Note that coverage is defined such that one has coverage if the reliability requirement is fulfilled. Also, energy consumption can be further optimized using these models.

Furthermore, the measurement setup can serve as a tool to develop better models in the future, as the results of this thesis show the lack of the current

models. The unique features of this setup is that it is completely waterproof and can last for two weeks at sea when mounted to a buoy. This can be particularly useful for measuring the fading of the channel over a longer time, and to test the impact of different sea state and weather conditions. The system is also ready to work with the 2.4 GHz LoRa technology, that can be an alternative to the one working at 868 MHz.

Chapter 7
Future work

This chapter will first discuss the limitations and possible improvements of the measurement setup. Next, some directions will be given for the future channel modeling propagation at sea for low antenna height applications.
Measurement setup:

- The sensitivity of the LoRa transceiver used in this setup is 24 dB lower than the reported value. This limits the range of the setup and prevents measuring the effect of the diffraction loss.
- So far, the power consumption of the setup was not optimized. Improvements could make the setup last longer when mounted on a buoy at sea.
- For the slave box, the same dipole antenna was used as for the master box. When installed at the coastline, the slave box can also receive multipath components that come from the surrounding buildings, which could affect the path loss measurement. This could be solved by using a directional antenna instead.

Channel modeling at sea:

- Conducting similar measurements at larger distances and different routes
- Validating the model for the diffraction loss [23] by measuring at distances beyond LOS.

Note that only one path loss model is studied in the theoretical investigation. There is of course a lot of other research, focusing more on radar systems and ship communication, from which the results could be interesting in this new application area.

References

[1] Recommendation ITU-R P.527-5 (2019), "Electrical characteristics of the surface of the earth."

[2] "Spherical coordinate system," Apr 2020. [Online]. Available: https://en.wikipedia.org/wiki/Spherical_coordinate_system

[3] Semtech, "SX1276/77/78/79 - 137 MHz to 1020 MHz Low Power Long Range Transceiver", SX1276/77/78/79 datasheet, Jan. 2019.

[4] "Douglas sea scale," Oct 2019. [Online]. Available: https://en.wikipedia.org/wiki/Douglas_sea_scale

[5] "Nb-iot frequency bands in europe." [Online]. Available: https://www.everythingrf.com/community/nb-iot-frequency-bands-in-europe

[6] K. Yang, A. F. Molisch, T. Ekman, T. Røste, and M. Berbineau, "A round earth loss model and small-scale channel properties for open-sea radio propagation," *IEEE Transactions on Vehicular Technology*, vol. 68, no. 9, pp. 8449–8460, Sep. 2019.

[7] Statista Research Department, "Number of connected devices worldwide 2030," Feb 2020. [Online]. Available: https://www.statista.com/statistics/802690/worldwide-connected-devices-by-access-technology/

[8] J. Petajajarvi, K. Mikhaylov, A. Roivainen, T. Hanninen, and M. Pettissalo, "On the coverage of lpwans: range evaluation and channel attenuation model for lora technology," in *2015 14th International Conference on ITS Telecommunications (ITST)*, Dec 2015, pp. 55–59.

[9] L. Parri, S. Parrino, G. Peruzzi, and A. Pozzebon, "Low power wide area networks (lpwan) at sea: Performance analysis of offshore data transmission by means of lorawan connectivity for marine monitoring applications," *Sensors 2019*, vol. 19, no. 14, p. 3239, Jul. 2019.

[10] G. Callebaut, G. Leenders, C. Buyle, S. Crul, and L. V. der Perre, "Lora physical layer evaluation for point-to-point links and coverage measurements in diverse environments," in *2019 European Conference on Networks and Communications (Eu-CNC)*, 2019.

[11] Z. Zhang, S. Cao, and Y. Wang, "A long-range 2.4g network system and scheduling scheme for aquatic environmental monitoring," *Electronics*, vol. 8, no. 8, p. 909, 2019.

[12] R. G. Vaughan and J. B. Andersen, *Channels, Propagation and Antennas for Mobile Communications*, 2nd ed. Institution of Engineering and Technology, 2017.

[13] "Link budget," Jun 2020. [Online]. Available: https://en.wikipedia.org/wiki/Link_budget

[14] A. F. Molisch, *Wireless Communications*, 2nd ed. Wiley Publishing, 2011.

[15] Y. H. Lee, F. Dong, and Y. S. Meng, "Near sea-surface mobile radiowave propagation at 5 ghz: Measurements and modeling," *Radioengineering*, vol. 23, pp. 824–830, 09 2014.

[16] A. Habib and S. Moh, "Wireless channel models for over-the-sea communication: A comparative study," *Appl. Sci.*, vol. 9, no. 3, p. 443, 2019.

[17] K. Yang, T. Roste, F. Bekkadal, and T. Ekman, "Experimental multipath delay profile of mobile radio channels over sea at 2 ghz," in *2012 Loughborough Antennas Propagation Conference (LAPC)*, 2012, pp. 1–4.

[18] National Oceanic and Atmospheric Administration. Annual salinity at the surface. [Online]. Available: https://www.nodc.noaa.gov

[19] Y. Karasawa and T. Shiokawa, "Characteristics of l-band multipath fading due to sea surface reflection," *IEEE Transactions on Antennas and Propagation*, vol. 32, no. 6, pp. 618–623, June 1984.

[20] D. Barrick, "Rough surface scattering based on the specular point theory," *IEEE Transactions on Antennas and Propagation*, vol. 16, no. 4, pp. 449–454, 1968.

[21] B. Smith, "Geometrical shadowing of a random rough surface," *IEEE Transactions on Antennas and Propagation*, vol. 15, no. 5, pp. 668–671, 1967.

[22] F. Huang, X. Liao, and Y. Bai, "Multipath channel model for radio propagation over sea surface," *Wireless Personal Communications*, vol. 90, no. 1, pp. 245–257, 2016.

[23] K. Bullington, "Radio propagation at frequencies above 30 megacycles," *Proceedings of the IRE*, vol. 35, no. 10, pp. 1122–1136, 1947.

[24] Semtech Corporation, Appl. Note 1200.22.

[25] K. Mekki, E. Bajic, F. Chaxel, and F. Meyer, "A comparative study of lpwan technologies for large-scale iot deployment," *ICT Express*, vol. 5, no. 1, pp. 1 – 7, 2019. [Online]. Available: http://www.sciencedirect.com/science/article/pii/S2405959517302953

[26] "Deployment map." [Online]. Available: https://www.gsma.com/iot/deployment-map/

[27] ERC Recommendation 70-3, "Relating to the use of short range devices (srd)."

[28] M. Lauridsen, H. Nguyen, B. Vejlgaard, I. Z. Kovacs, P. Mogensen, and M. Sorensen, "Coverage comparison of gprs, nb-iot, lora, and sigfox in a 7800 km2 area," in *2017 IEEE 85th Vehicular Technology Conference (VTC Spring)*, 2017, pp. 1–5.

Printed by Tryckeriet i E-huset, Lund 2020

LUND
UNIVERSITY

Series of Master's theses
Department of Electrical and Information Technology
LU/LTH-EIT 2020-778
http://www.eit.lth.se